DOKUZ EYLUL UNIVERSITY

GRADUATE SCHOOL OF NATURAL AND APPLIED SCIENCES

PHYSICAL AND ELECTROCHEMICAL CHARACTERIZATION OF CO-DEPOSITED TiO_2 AND MgO LAYER ON Ti6AI4V BY MICRO ARC OXIDATION (MAO)

by

Alper KAYA

June, 2011

İZMİR

PHYSICAL AND ELECTROCHEMICAL CHARACTERIZATION OF CO-DEPOSITED TiO_2 AND MgO LAYER ON Ti6AI4V BY MICRO ARC OXIDATION (MAO)

A Thesis Submitted to the Graduate School of Natural and Applied Sciences of Dokuz Eylul University in Partial Fulfillment of the Requirements for the Master of Science in Metallurgy and Materials Engineering, Metallurgy and Materials Engineering Program

by

Alper KAYA

June, 2011

İZMİR

M. Sc THESIS EXAMINATION RESULT FORM

We have read the thesis entitled **"PHYSICAL AND ELECTROCHEMICAL CHARACTERIZATION OF CO-DEPOSITED TiO_2 AND MgO LAYER ON Ti6AI4V BY MICRO ARC OXIDATION (MAO)"** completed by **ALPER KAYA** under supervision of **PROF.DR. AHMET ÇAKIR** and we certify that in our opinion it is fully adequate, in scope and in quality, as a thesis for the degree of Master of Science.

Prof. Dr. Ahmet ÇAKIR

Supervisor

Prof. Dr. Mustafa GÜDEN

(Jury Member)

Prof. Dr. Hasan YILDIZ

(Jury Member)

Prof. Dr. Mustafa SABUNCU

Director

Graduate School of Natural and Applied Sciences

ACKNOWLEDGEMENTS

I sincerely thank for the people who mentally support and encourage me, aid me in my pursuing of the M. Sc. degree, and help in my academic accomplishment.

I cordially would like to express my thanks to my supervisor, Prof. Dr. Ahmet ÇAKIR for his guidance, interest and encouragement.

I also would like to thank my all colleagues especially my project partner Güler UNGAN for her cooperation and friendship.

Finally, I would like to thank my family for their support and persistence.

Alper KAYA

PHYSICAL AND ELECTROCHEMICAL CHARACTERIZATION OF CO-DEPOSITED TiO_2 AND MgO LAYER ON Ti6AI4V BY MICRO ARC OXIDATION (MAO)

ABSTRACT

Although Mg has limited amount in natural bone structure; its presence is vital for bone growth. The intention of this study is to obtain a composite oxide layer which is porous, well-adherent and integrated with elemental or oxide form of Mg inside titanium oxide on the surface of Ti6Al4V. It is expected that integration of Mg in titanium oxide on Ti6Al4V surface will develop this biocompatibility properties. The porous layer which will be formed by MAO will cause a strong adhesion of the implant and bone. Finally the presence of Mg in MAO modified coating on implant materials will improve the bioactivity of the implant in vivo conditions.

Phase identifications of the fabricated coatings were performed by Rigaku D/max-2200/PC XRD (X-ray diffractometer) and surface morphologies were investigated using JEOL-JJM 6060 model SEM (scanning electron microscopy) with an EDS (energy dispersive X-ray spectroscopy) system attachment. Surface roughness of coatings was analyzed by XP2 surface profilometry (Ambios XP2 Stylus Profiler). Electrochemical characterization of coatings was analyzed with potentiostat/galvanostat (Gamry Reference 3000 Potentiostat/Galvanostat/ZRA). It was shown that Mg was doped into the titanium oxide and a new phase, magnesium dititanate had been obtained. The structure of coatings was porous and doped with Mg at concentration between 2.35 - 7.05 percent.

Keywords: Micro arc oxidation, electrochemical characterization, co-deposition, biocompatibility, bioactivity.

Ti6AI4V ÜZERİNDE MİKRO ARK OKSİTLENME (MAO) İLE BİRLİKTE ÇÖKTÜRÜLEN TiO_2 VE MgO TABAKASININ FİZİKSEL VE ELEKTROKİMYASAL KARAKTERİZASYONU

ÖZ

Mg, doğal kemik yapısında eser miktarda olmasına rağmen, varlığı kemik gelişiminde önem teşkil etmektedir. Bu çalışmanın amacı, Ti6Al4V üzerine Mg' un elementel ya da oksit formunda titanium oksit ile gözenekli, sıkıca yapışan ve tümleşen şekilde birlikte çöktürülerek kompozit bir tabaka elde edilmesidir. Mg' un Ti6Al4V alaşım yüzeyinde oluşan titanium oksit ile birleştirilmesinin biyouyumluluk özelliğini geliştirmesi beklenmektedir. MAO ile oluşturulmuş gözenekli tabaka, kemik ve implantın sıkıca kaynaşmasına sebep olacaktır. Son olarak MAO modifiye edilmiş kaplamaların içindeki Mg varlığı, vücut içi ortamlarda implantın biyoaktivitesini geliştirecektir.

Elde edilen kaplamaların faz tanımlamaları Rigaku D/max-2200/PC XRD (X-ray diffractometer) ile; yüzey morfolojileri ve elementel analizler JEOL-JJM 6060 model SEM ve EDS (energy dispersive X-ray spectroscopy) sistem eklentisi ile; yüzey pürüzlülükleri ise XP2 yüzey profilometresi (Ambios XP2 Stylus Profiler) ile belirlenmiştir. Kaplamaların elektrokimyasal karakterizasyonları Gamry Reference 3000 model Potansiyostat/Galvanostat ile gerçekleştirilmiştir. Çalışmalar neticesinde Mg' un titanium oksit içine doplandığı ve magnezyum dititanat fazının elde edildiği sonucuna varılmıştır. Kaplamaların yapıları gözeneklidir ve yüzde 2.35-7,05 Mg içermektedir.

Anahtar kelimeler: Mikro ark oksitleme, elektrokimyasal karakterizasyon, birlikte çöktürme, biyouyumluluk, biyoaktivite.

CONTENTS

Page

CHAPTER ONE

INTRODUCTION

Biomaterials have been used in human body since 1900's. They are manufactured to heal or replace a tissue of body. For this aim, there are many requirements for them to be used as a metallic implants in living tissue. Some of these requirements are corrosion resistance, toxicity, biocompatibility, bioactivity, mechanical and chemical properties.

All around the world, the most used metallic biomaterial is titanium and its alloys. They are preferred for their high strength/density ratio, high corrosion resistance via their protective oxide, bioactivity, biocompatibility and cytocompatibility (compatibility with respect to toxicity) properties.

There is no naked surface of a biomaterial in a living tissue since they are coated either physiologically *in vivo* conditions or physically forming an interface on implants. Interface between host tissue and implant is vital for the future of both implant and patience. To improve the properties of this interface, many surface technologies have been developed. Among them, micro arc oxidation (plasma electrolytic oxidation) is recently used because of its inherent feature such as high adherence to the substrate, porosity and corrosion protection. A porous oxide layer on an implant surface is manufactured to increase the surface-tissue contact area enabling its bonding ability to host tissue to increase.

Mg is a trace element of human body amounting nearly 19 g (Lentner, C. (Ed.), *Geigy Scientific Tables*, Ciba-Geigy, Basle, 1981.). The importance of Mg is that; the bone can grow in presence of it faster than when it lacks. Lack of magnesium causes bone osteogenesis and termination of bone growth.

Among the studies where titanium or titanium alloys has been treated with micro arc oxidation (MAO), it was shown that bioactivity, biocompatibility have been developed and improved. Most of the surfaces produced as such were found

successful for the creation of apatites *in vivo* conditions (Chen, Shi, Wang, Yan, 2006), (Kim, Ryu, Sung, 2007).

In view of the ongoing discussion, we aimed to dope Mg into TiO_2 by MAO. For this purpose, predetermined composition of electrolytes consisting of Mg-acetate-tetrahydrate, Ca-glicerophosphate hydrate, with (electrolyte No.2) and without (electrolyte No.3) Ca-acetate-hydrate have been used to study the formation of an oxide layer under the scrutiny of various time intervals and currents. Electrolytes have included Ca element also. Electrochemical coating of $Mg(OH)_2$ before MAO treatment was carried out to investigate the success of pre-MgO coating in producing composite oxide layers, the main component of which is TiO_2. $Mg(OH)_2$ was heat treated to convert it to MgO. Following surface treatments, various characterization techniques have been applied to surfaces. Corrosion test of surfaces have been carried out in 0.9% NaCl solution. The results of scanning electron microscopy (SEM), X ray diffraction (XRD), surface profilometry (XP2), electron dispersive spectroscopy (EDS), Tafel extrapolation and optical micrographs show that the oxide layer of the surfaces was porous and oxide was modified with the insertion of Mg. SEM micrographs of MAO surfaces obtained in electrolyte No.2 have shown an increase in pore size while decreasing number of pores with increasing current. Phase structure of surfaces was found to consist of rutile, $MgTi_2O_5$ and $CaTi_4O_9$. Crystallinity of the phases was depended on electrolyte composition and concentration, current and time parameters. EDS studies showed that Mg content in the MAO modified surfaces varied up to 7.05% depending on bath composition and test parameters such as current and time. Mg content in MAO oxide was found to decrease both in electrolytes No.2 and No.3, in cases where surfaces were pre-coated with MgO. No specific trends were found in surface roughness regarding MAO parameters tested in this study. Polarization resistances of the surfaces have shown that, MAO parameters are effective for controlling dissolution properties of the surfaces in NaCl solution. Increase in current for MAO treatment seemed to have decreased polarization resistance indicating the increase in dissolution properties of the Mg-modified MAO film produced in electrolyte No.3. The MAO modified surfaces maintained their porosity following corrosion test.

CHAPTER TWO

METALLIC IMPLANTS IN GENERAL

The first developed metal used in human body was “Sherman Vanadium Steel” which was used to produce bone fracture plates and screws. Ion release (Fe, Cr, Co, Ni, Ti, Ta, Mo and W) from metal implants could be tolerated by the body in minute amount. Natural occurring forms of these elements are important but large amount of them cannot be tolerated by human body. For example iron (Fe) is main element of bone cell functions; Co is required for synthesis of B_{12} vitamin; and copper (Cu) is a necessity for the cross linking of elastin in the aorta. The main importance of biomaterials is the corrosion behavior of them in human body. Lack of corrosion resistance of these device can initiate some kind of disease which may result in the lost of host tissue. And also some kind of alloying elements can be toxic in human body; this circumstance of them can result of carcinoma. These drawbacks are the main reasons to design and modify an implant to develop biocompatibility and bioactivity (Park, Kim, 2007)

Mechanical properties of biomaterials are also important. An implant should safely work under skeletal stresses. Especially young modulus, hardness, fatigue limit, friction and yield strength are main mechanical characteristics of them to determine whether they are suitable for this usage or not.

There are mainly three groups of metallic implants which are manufactured for orthopedic usage: Stainless steels, Co-Cr alloys and Ti alloys.

Table 2.1 Classification of biomaterials (Teoh, 2004).

Biological Materials	Synthetic Biomedical Materials
1. Soft Tissue Skin, Tendon, Pericardium, Cornea	**1. Polymeric** Ultra High Molecular Weight Polyethylene (UHMWPE), Polymethylmethacarylate (PMMA), Polyethyletherketone (PEEK), Silicone, Polyurethane (PU), Polytetrafluoroethylene (PTFE)
2. Hard Tissue Bone, Dentine, Cuticle	**2. Metallic** Stainless Steel, Cobalt-based Alloy (Co-Cr-Mo), Titanium Alloy (Ti-Al-V), Gold, Platinum
	3. Ceramic Alumina (Al_2O_3), Zirconia (ZrO_2), Carbon, Hydroxylapatite [$Ca_{10}(PO_4)_6(OH)_2$], Tricalcium Phosphate [$Ca_3(PO_4)_2$], Bioglass [$Na_2O(CaO)(P_2O_3)(SiO_2)$], Calcium Aluminate [$Ca(Al_2O_4)$]
	4. Composite Carbon Fiber (CF)/PEEK, CF/UHMWPE, CF/PMMA, Zirconia/Silica/BIS-GMA

Before manufacturing an implant, it is very important to decide the kind of the material according to the property of the host tissue. Table 2.1 gives us the preferential of the implant materials according to the kind of tissues. Polymeric biomaterials are usually utilized for soft tissues such as skin, tendon, cornea; metallic, ceramic or composite biomaterials are for hard tissues such as bone. The aim of the researches for manufacturing implants is to obtain the same tissue properties from biomaterials. These properties are related with mechanics, chemistry and biology.

Young modulus of biomaterials has a vital importance for bone grafts. After implantation of a biomaterial to bone, stress is applied to host tissue and implant according to their young modulus. The bone is very interesting tissue that it can be exposed to necrosis in the lack of stress on it. This type of tissue grows by stress. Lately there is no implant material which performs the same physical property such as bone. Every kind of implants has higher young modulus than natural bone. This problem is the main reason for biomedical search and development studies. Various mechanical properties of biomaterials are given in Figure 2.1 – 2.4.

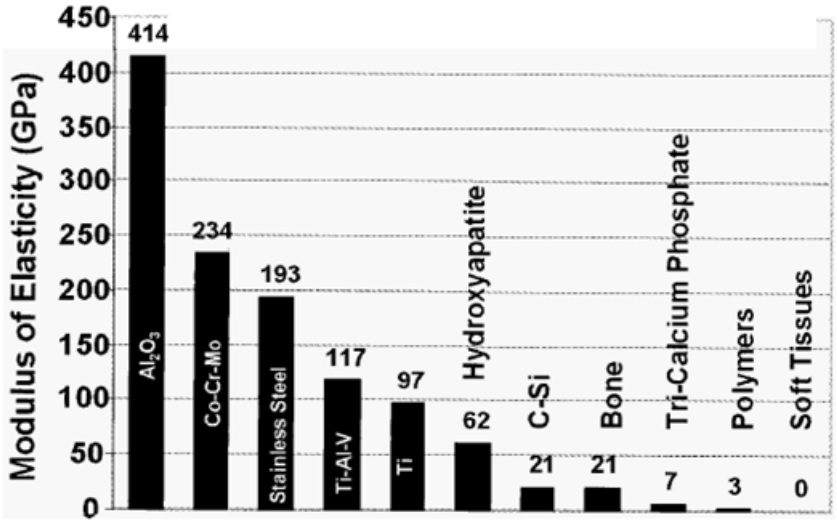

Figure 2.1 Comparison of modulus of elasticity of biomaterials. Note the very high values for ceramics and metals. Titanium has the closest young modulus to natural bone in metallic implant materials (Teoh, 2004).

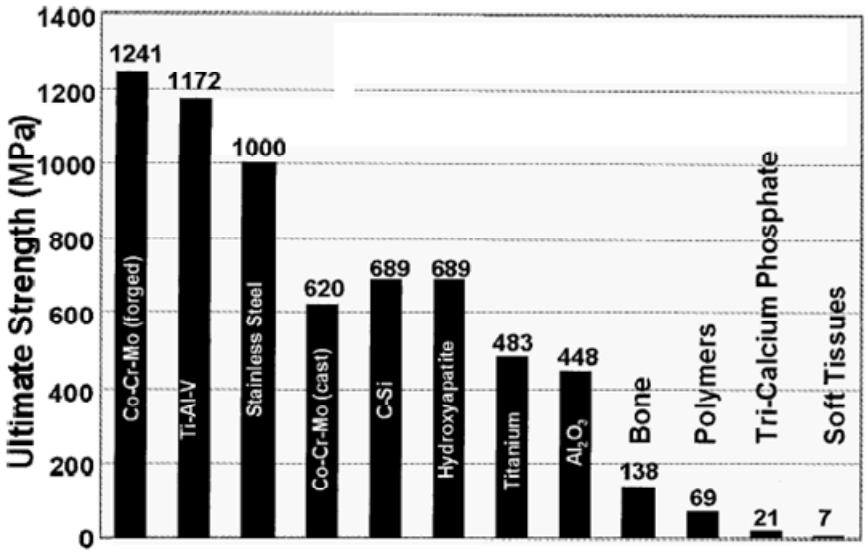

Figure 2.2 Comparison of ultimate tensile strengths of biomaterials. Note the exceptionally high values for metals which make the metals an ideal choice for load bearing applications (Teoh, 2004).

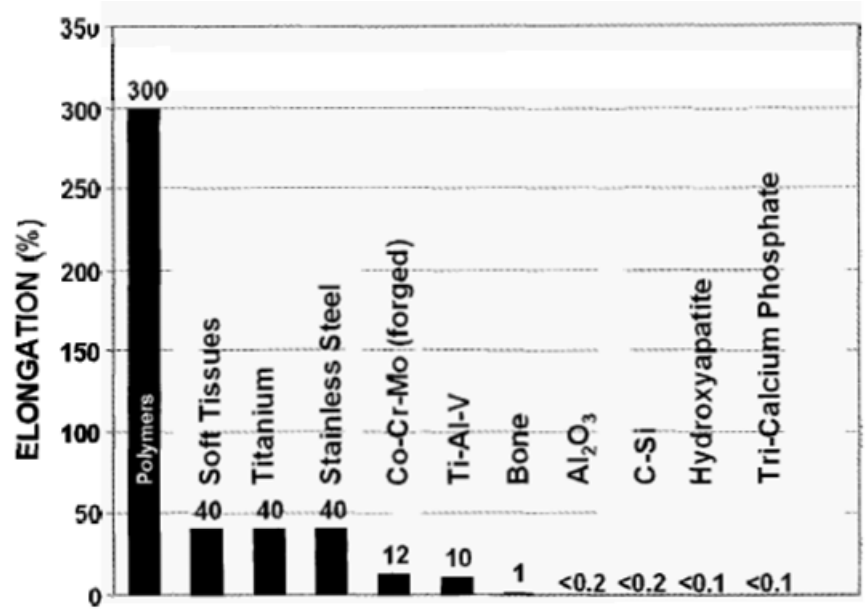

Figure 2.3 Comparison of elongation at failure of biomaterials. Note that polymers have exceptional elongation as compared to other materials. This is a measure of their high ductility (Teoh, 2004).

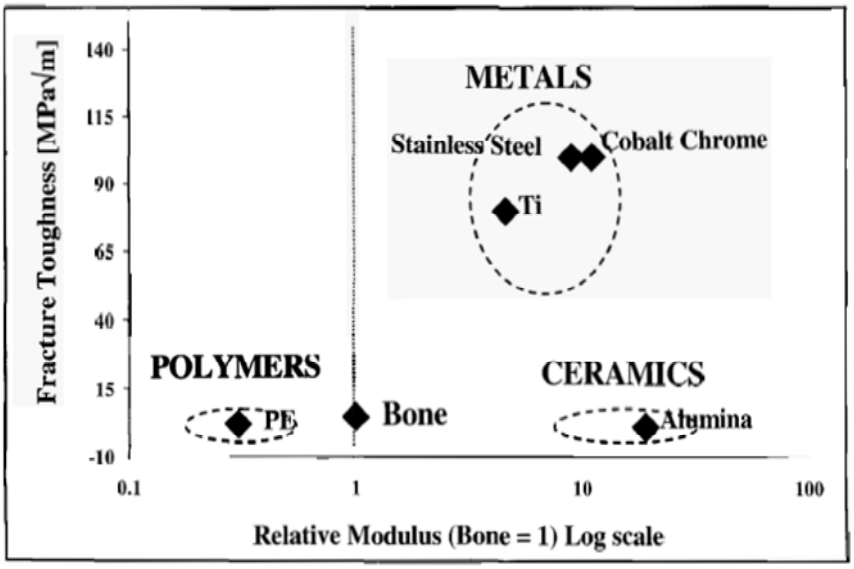

Figure 2.4 Comparison of fracture toughness of biomaterials relative to the log (Young's modulus) with bone as the reference. Note that the fracture toughness values of metals are generally several orders of magnitude higher than those of the other materials. The Young's modulus is also much higher than that of bone, giving rise to stress shielding (Teoh, 2004).

Corrosion characteristics of some metallic implant materials are given in Table 2.2.

Table 2.2 Electrochemical properties of some metallic implants (corrosion resistance) in 0.1 M NaCl at pH=7 (Black, Levine, Jacobs, 2007)

Alloy	**ASTM designation**	**Density (g/cm^3)**	**Corrosion potential (vs calomel - mV)**	**Passive current density (mA/cm^2)**	**Breakdown potential (mV)**
Stainless steel	F 138	8.0	-400	0.56	200-770
Co-Cr-Mo	F 75	8.3	-390	1.36	420
Ti; Cp-Ti Ti-6Al-4V	 F 67 136	 4.5 4.43	 -90 to -630 -180 to -510	 0.72- 9.0 0.9- 2.0	 >2.000 >1.500

2.1 Stainless Steels

The most common stainless steel used in orthopedic application is Grade 2 (ASTM F138), which is also known as 316 steel. In 1950's, the carbon concentration of 316 steel was reduced for better corrosion resistance. So it became known as

316L. In the presence of high C concentration, there is a tendency for carbon to interact with chromium to form chromium carbide which is brittle and segregate at the grain boundaries. As a result weakening of the corrosion resistance of the stainless steel implants occurs invariable. Chemical compositions of stainless steels are given in Table 2.3.

Table 2.3 Chemical compositions of some stainless steels (Sarıtaş, 2004)

ASTM	EN Material No.	Chemical Composition, weight % (max.)									
		C	Mn	Si	P	S	Cr	Ni	Mo	N	Others
Ferritic Stainless Steels											
409	1.4512	0.08	1.0	1.00	0.045	0.03	10.5-11.75	-	-	-	(6xC)Ti
430	1.4016	0.12	1.0	1.00	0.04	0.03	16.0-18.0	-	-	-	-
430Ti	(1.450)	0.10	1.0	1.00	0.04	0.03	16.0-19.5	0.75	-	-	(5xC)Ti
439	1.4510	0.07	1.0	1.00	0.04	0.03	17.0-19.0	0.5	-	-	0.2+ 4(C+N)Ti
Martensitic Stainless Steels											
410	1.4006	0.15	1.0	1.00	0.04	0.03	11.5-13.0	-	-	-	-
420	1.4021	0.15min	1.0	1.00	0.04	0.03	12.0-14.0	-	-	-	-
440A	-	0.6-0.75	1.0	1.00	0.04	0.03	16.0-19.5	-	0.75	-	-
440C	1.4125	0.95-1.2	1.0	1.00	0.04	0.03	16.0-18.0	-	0.75	-	-
Dublex Stainless Steels											
2205*	1.4462	0.03	2.0	1.0	0.03	0.02	21.0-23.0	4.5-6.5	2.5-3.5	0.08-0.2	-
329	1.4460	0.20	1.0	0.75	0.04	0.03	23.0-23.0	2.5-5.0	1.0-2.0	-	-
Austenitic Stainless Steels											
201	1.4372	0.15	5.5-7.5	1.00	0.06	0.03	16.0-18.0	3.5-5.5	-	0.25	-
301	1.4310	0.15	2.0	1.00	0.045	0.03	16.0-18.0	6.0-8.0	-	-	-
304	1.4301	0.08	2.0	1.00	0.045	0.03	18.0-20.0	8.0-10.5	-	-	-
304L	1.4306	0.03	2.0	1.00	0.045	0.03	18.0-20.0	8.0-12.0	-	-	-
304LN	1.4311	0.03	2.0	1.00	0.045	0.03	18.0-20.0	8.0-12.0	-	0.1-0.16	
309	1.4828	0.20	2.00	1.00	0.045	0.03	22.0-24.0	12.0-15.0			
309S	1.4833	0.08	2.00	1.00	0.045	0.03	22.0-24.0	12.0-15.0			
310	1.4841	0.25	2.00	1.50	0.045	0.03	24.0-26.0	19.0-22.0			
310S	1.4845	0.08	2.00	1.50	0.045	0.03	24.0-26.0	19.0-22.0			
316	1.4401	0.08	2.00	1.00	0.045	0.03	16.0-18.0	10.0-14.0	2.0-3.0		
316L	1.4404	0.03	2.00	1.00	0.045	0.03	16.0-18.0	10.0-14.0	2.0-3.0	-	-
316LN	1.4406	0.03	2.00	1.00	0.045	0.03	16.0-18.0	10.0-14.0	2.0-3.0	0.1-0.16	
316Ti	1.4571	0.08	2.00	1.00	0.045	0.03	16.0-18.0	10.0-14.0	2.0-3.0	-	5x(C+N)Ti
321	1.4541	0.08	2.00	1.00	0.045	0.03	17.0-19.0	9.0-12.0	-	-	(5xC)Ti
347	1.4550	0.08	2.00	1.00	0.045	0.03	17.0-19.0	9.0-13.0	-	-	(10xC)Nb
Age Hardenable Stainless Steels											
631	1.4568	0.09	1.0	1.0	0.04	0.04	16.0-18.0	6.5-7.5	-	-	0.75-1.5Al
632	1.4535	0.09	1.0	1.0	0.04	0.03	14.0-16.0	6.5-7.5	2.0-3.0	-	0.75-1.5Al

*Commercial name

2.1.1 Types and Properties of Stainless Steels

Chromium is the major component of a stainless steel to increase the corrosion resistance. At least 11% chromium compositions are required to manufacture an effective stainless steel. Because of chromium is a more active element than iron, the oxide form of chromium can protect the main structure of steel from propagation of corrosion into the bulk.

Austenitic stainless steels are the most common steels which are used in orthopedic surgery. Especially 316 or 316L types are preferred for this usage. These types can be hardened only by cold-working. Some kind of alloying elements determine the phase structures of stainless steels. Especially Ni stabilizes austenite phase and Cr stabilizes ferrite phase at room temperature. Phase transition curves change by adding alloying elements to the structure. Austenite phase is non-magnetic, so it is better for corrosive mediums than the other type of phases. And also small amount of molybdenum in stainless steels provide pitting corrosion resistance in salt water. Figure 2.5 shows the effect of Cr or Ni concentration on the structure of stainless steel which includes 0.1 w/o C.

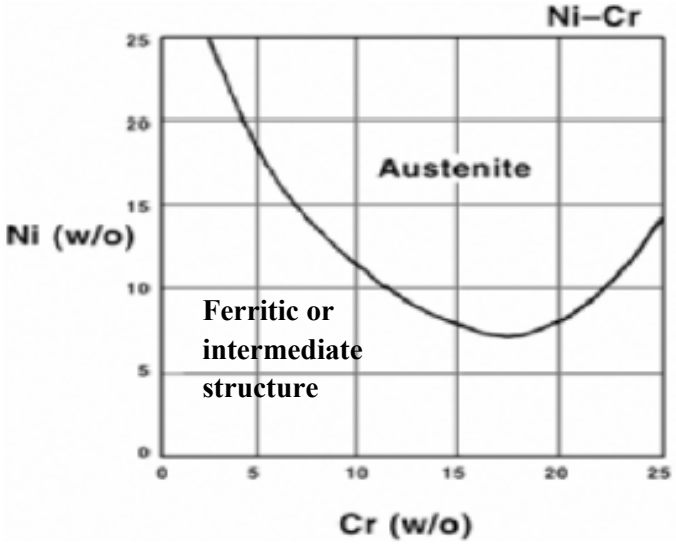

Figure 2.5 Effect of Ni and Cr contents on the austenitic phase of stainless steels containing 0.1 w/o C. Reprinted with permission from Keating (1956). Copyright © 1956, Butterworths

Generally, properties of stainless steels depend on heat-treatment and cold working ability of them. Heat treatment is preferred to soften the materials and cold-working is for increasing strength and hardness. 316 L stainless steel may corrode inside the body under highly stressed and oxygen-depleted region. Two main drawback of this type of steels are the vulnerability of their crevice and stress corrosion in body. Therefore these types of biomaterials are not preferred for permanent implants. They are usually manufactured for temporary parts such as plates, screws and nails.

As shown in Figure 2.6, austenitic stainless steels work-harden very rapidly. That is why they cannot be cold-worked without intermediate heat treatments. This heat treatment should not initiate the formation of chromium carbide (Cr_4C) at the grain boundaries. This formation causes depletion of Cr in grains so insufficient Cr content causes the corrosion resistance to decrease. Welding ability of austenitic stainless steels is not adequate with respect to other steels.

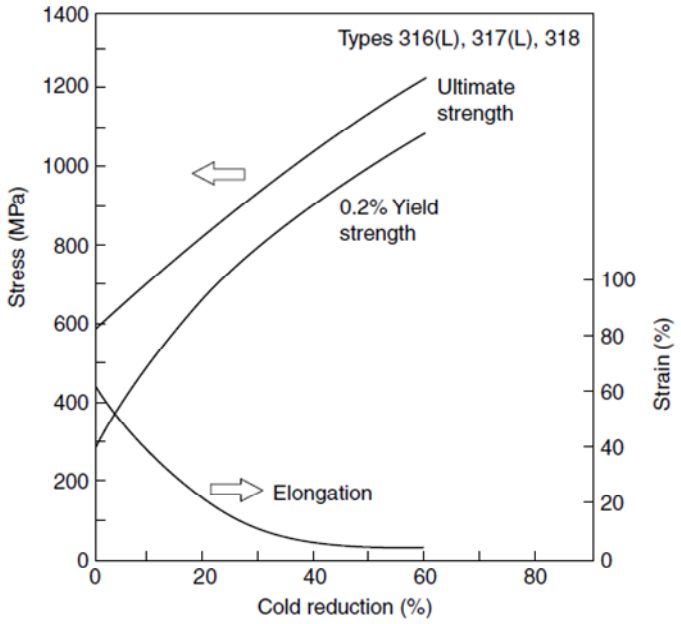

Figure 2.6 Effect of cold-working on the yield and ultimate tensile strength of 304 stainless steel (ASM, 1978).

Table 2.4- 2.7 give the standards, properties and usage areas of some stainless steels.

Table 2.4 Standards and properties of 304, 304 L, 304LN, 309/309S stainless steels (Sarıtaş, 2004):

ASTM Standard	**304**	**304L**	**304LN**	**309/309S**
Class	**Austenitic**	**Austenitic**	**Austenitic**	**Austenitic**
Yield Strength 0,2 % (MPa)	At least 200(annealed) Till 500 (cold rolled)	At least 190(annealed) Till 500 (cold rolled)	At least 270(annealed)	At least 230 (309) At least 210 (309S)
Young Modulus (MPa)	200	200	200	200
Tensile Strength (MPa)	500 (annealed) 700 (cold rolled)	470 (annealed) 660 (cold rolled)	550-750	500-750 (309) 500-750 (309S)
Hardness^{max} (HRB) (ASTM A-240)	201	201	207	217 (309) / 217 (309S)
Cold-working Ability	Very Good	Very Good	Very Good	Very Good
Machining Ability	Via convenient tool and cooling	Via convenient tool and cooling	Via convenient tool and cooling	Via convenient tool and cooling
Corrosion Resistance	Perfect atmospheric corrosion resistance in notr dry air without humidity	Corrosion endurance is similar to 304. Additionally resistive to intergranular corrosion and stress corrosion crack. Suitable for nitric acid including atmosphere.	Corrosion endurance is similar to 304. Additionally by adding nitrogen to structure, increasing mechanical properties.	Against sulphur including gases: medium (309), low (309S). Against nitrogen including gases: Perfect (309), low(309S)
Usage Areas	House goods, architectural and automotive devices.	Similar to 304. Used for the parts which cannot be annealed after welding? Especially concentrated nitric acid including atmosphere	Similar to 304L. Better mechanical properties. Can be used till 400°C permanently in service. Suitable for the pressured tanks for chemistry.	Used for heat resistance required applications. Construction for furnace, radiator, cementation box, annealing furnaces e.g.

Table 2.5 Standards and properties of 310/310S, 316, 316L, 316Ti stainless steels (Sarıtaş, 2004):

ASTM Standard	**310/310S**	**316**	**316L**	**316Ti**
Class	**Austenitic**	**Austenitic**	**Austenitic**	**Austenitic**
Yield Strength 0,2 % (MPa)	At least 230(310) At least 210(310S)	At least 210(annealed) Till 500 (cold rolled)	At least 200(annealed) Till 450 (cold rolled)	At least 220 (annealed) Till 700 (cold rolled)
Young Modulus (MPa)	200	200	200	200
Tensile Strength (MPa)	550-800 (310) 500-750 (310S)	510 (annealed) 610 (cold rolled)	500 (annealed) 600 (cold rolled)	540-700 (annealed) Till 700 (cold rolled)
Hardness^{max} (HRB) (ASTM A-240)	217 (310)/ 217 (310S)	217	217	217
Cold-working Ability	Very Good	Very Good	Very Good	Very Good
Machining Ability	Via convenient tool and cooling	Via convenient tool and cooling	Via convenient tool and cooling	Via convenient tool and cooling
Corrosion Resistance	Against sulphur including gases: low (310), medium-low (310S). Against nitrogen including gases: Perfect	Corrosion endurance is developed by molybdenum addition. Pitting and crevice corrosion behaviour are better. Can be used in air, industrial atmosphere and sea water in safe.	Similar to 316. Additionally Sensitivity of intergranular corrosion does not occur. Can be used in oxidizing acids, sea water and the other pitting corrosion probable areas.	Similar to 316. Sensitivity of intergranular corrosion does not occur in case of stabilizing of internal structure by Titanium. Can be used till 400°C permanently even welded.
Usage Areas	Heat resistive applications. Furnace construction, stem vessels, thermal components in petroleum industry	Suitable for excessive aggressive atmospheres. Used in chemistry, petro-chemistry and food industry. . Can be used till 300°C in heat converters, steam vessels, kitchens permanently.	Similar to 316L. Preferred for the parts which will not be welded after heat treatment.	Similar to 316L. Additionally high temperature properties are good. Can be used till 400°C without any intergranular corrosion danger. Preferred in chemistry, petro-chemistry, coal, cellulose, textile, dye photograph, resin and rubber industry.

Table 2.6 Standards and properties of 321, 409, 420, 430 stainless steels (Sarıtaş, 2004):

ASTM Standard	**321**	**409**	**420**	**430**
Class	**Austenitic**	**Ferritic**	**Martensitic**	**Ferritic**
Yield Strength 0,2 % (MPa)	At least 205(annealed) Till 450 (cold rolled)	At least 220(annealed) Till 350 (cold rolled)	450(annealed)	At least 210 (annealed)
Young Modulus (MPa)	200	220	216	220
Tensile Strength (MPa)	520 (annealed) 720 (cold rolled)	380 (annealed) 420 (cold rolled)	650-800 (annealed) 1570 (after quenching) 930 (quenching+650°C temp.) 750 (quenching+750°C temp.)	430-600 (annealed)
Hardness^{max} (HRB) (ASTM A-240)	217	179	180	183
Cold-working Ability	Very Good	Good	-	Good
Machining Ability	Via convenient tool and cooling	Such as soft steels	Such as soft steels when annealed	Such as soft steels
Corrosion Resistance	Perfect. Similar to 304. Sensitivity of intergranular corrosion does not occur in case of stabilizing of internal structure by Titanium. Sensitive to stress corrosion cracking	Performs a good corrosion resistance against air, water and lots of chemicals.	Good endurance against diluted acids. Sensitive to chlorides especially in oxidizing atmosphere.	Adequate corrosion resistance in atmosphere, non-chloride including aqueous atmosphere and alkaline solutions. Durable for sulphur including gases of coal and petroleum fueled furnaces.
Usage Areas	Durable for corrosion even that is not welded and annealed. No intergranular corrosion till 400°C. Ductile at low temperatures. Preferred for drug, photograph, food industry; store construction and fittings.	Generally preferred for the constructions where galvanized steels are not adequate. Can be used for pipes and heat converters in chemistry and petro-chemistry, kitchen devices and sport equipments.	Preferred for high strength and friction resistance required parts. Brittle. Blades, medical devices, mold parts, brake discs, valves e.g.	Has a ferritic stainless steel quality for general purpose. Automotive industry, kitchen parts and architecture are some kind of application areas.

Table 2.7 Standards and properties of 439(430Ti), 2205 stainless steels (Sarıtaş, 2004):

ASTM Standard	439 (430Ti)	2205
Class	**Ferritic**	**Ferritic-ostenitic (duplex)**
Yield Strength 0,2 % (MPa)	At least 240(annealed)	At least 240(annealed)
Young Modulus (MPa)	220	200
Tensile Strength (MPa)	430-600 (annealed)	640-900 (annealed)
Hardness^{max} (HRB) (ASTM A-240)	183	293
Cold-working Ability	Good	Good
Machining Ability	Such as soft steels	Via convenient tool and cooling
Corrosion Resistance	Better than 430 quality. Internal structure is stabilized via Titanium. No sensitization for stress corrosion. Has a good corrosion resistance in temperature changing circumstance.	Has a good corrosion resistance against accustomed corrosion types.
Usage Areas	Common usage areas by means of welding ability and ductility. Can be used for water heaters, exhaust systems, washing machines and food establishment.	Chemistry, petro-chemistry, off-shore applications, pipe lines, stress bearing parts, pressure containers.

2.1.2 Oxide of Stainless Steels

Composition of surface oxide films on stainless steels are well understood in the field of engineering. In an austenitic stainless steel, the surface oxide film consists of iron, chromium and a small amount of molybdenum. But it does not contain nickel while in the air and in chloride solutions (Bruesch, Muller, Atrens, Neff, 1985), (Jin & Atrens, 1987).

On the other hand, surface oxide film on 316 L steel polished mechanically in de-ionized water consists of oxide species of iron, chromium, nickel, molybdenum and manganese and its thickness is about 3.6 nm (Hanawa, Hiromoto, Yamamoto, Kuroda, 2002).

2.2 Co Based Alloys

Co-Cr alloys consist of ASTM F75 alloy which is produced via casting, ASTM F799 alloy which is produced via forging, ASTM F90 and ASTM F536 alloys whose mechanical properties are enhanced perfect by cold working. Mainly, these Co-based alloys include Cr such as stainless steels to increase the corrosion resistance. Chromium oxide layer, which is a product of corrosion of chromium, can isolate the bulk material from oxidizing atmosphere. This oxide layer is well adherent to the structure.

F 75 type of Co based alloys is generally used for dental applications and artificial joints; F 90 and F 1537 alloys are suitable for stem of prosthesis of heavily loaded joints (Buckwalter, Einhorn, Simon, 2000)

2.2.1 Types and Properties of Co-based Alloys

Table 2.8 gives the chemical compositions of some Co-Based alloys.

Table 2.8 Chemical Compositions of Co-Based Alloys for Surgical Implants (ASTM, 2000)

	Co28Cr6Mo (F 75) Castable		Co20Cr15W10Ni (F 90) Wrought		Co28Cr6Mo (F 1537) Wrough		Co35ni20Cr10Mo (F 562)	
Element	Min.	Max.	Min.	Max.	Min.	Max.	Min.	Max.
Cr	27.0	30.00	19.00	21.00	26.0	30.0	19.0	21.0
Mo	5.0	7.00	-	-	5.0	7.0	9.0	10.5
Ni	-	2.5	9.00	11.00	-	1.0	33.0	37.0
Fe	-	0.75	-	3.00	-	0.75	9.0	10.5
C	-	0.35	0.05	0.15	-	0.35	-	0.025
Si	-	1.00	-	1.00	-	1.0	-	0.15
Mn	-	1.00	-	2.00	-	1.0	-	0.15
W	-	0.20	14.00	16.00	-	-		
P	-	0.020	-	0.040	-	-	-	0.015
S	-	0.010	-	0.030	-	-	-	0.010
N	-	0.25	-	-	-	0.25	-	-
Al	-	0.30	-	-	-	-	-	-
Bo	-	0.01	-	-	-	-	-	0.015
Ti							-	1.0
Co	Balance							

F 75 alloys are used to produce porous coatings which are for biologic fixation of orthopedic implants. The porosity of the coating depends on the microstructure of substrate and the parameters of the coating process. If any sintering process is carried out on Co-based alloys; the sintering temperature should be determined well.

Because that point of temperature is vital parameter for fatigue limits of the substrate whose melting temperature is nearly 1225°C. Process required high temperature, causes the reduction of fatigue strength. After the strength concentration near the fixation areas of these porous coatings, the fatigue limit decreases till 200 MPa. After this condition, heat treatment is not an adequate solution to cope with this problem (Buckwalter, Einhorn, Simon, 2000).

Mechanical requirements of some Co-Based alloys are given in Table 2.9.

Table 2.9 Mechanical requirement of some Co-Based Alloys (ASTM, 2000)

Condition	Ultimate tensile strength min. (MPa)	Yield strength (0.2% offset) min. (MPa)	Fatigue strength (MPa)	Elongation min (%)	Reduction of area min(%)	Young Modulus (MPa)	Hardness (HB)
Co28Cr6Mo (F75) as cast	655	450	310	8	8	210	254-325
Co20Cr15W10Ni (F90) annealed	860	310	-	30	-	210	
Co28Cr6Mo (F1537) annealed	897	517	-	20	20	210	254
Co35Ni20Cr10Mo (F562) annealed	793	241	340	50.0	65.0	232	

The forging alloy, F 799 (yield strength 896-1200 MPa) has ultimate mechanical properties compared to casting alloys. Hot forging effectively decrease the grain size. Thermomechanic casting procedure causes the inducing of microstructural phases which contribute to developed material properties

F 90 and F 562 alloys gain important mechanical properties by more than 40% cold working. Alloying F 90 with W improves machining and cold working manufacturing.

Cold working of F 562 alloy provides additional energy for FCC phase to turn into HCP as fine platelets throughout microstructure. The combination of very fine grain size and dispersed platelet structure delay the plastic deformation of material. Additionally, the material provides homogeneous dispersion of very fine grain sized Co-Mo precipitations (Co_3Mo) which make the structure more durable via heat treatment. Finally the strongest material obtained among the other implant alloys. Scope, range, amount and easy fabrication of Co based alloys make them ideal for

orthopedic applications. Cr content of Co based alloys provides excellent corrosion resistance and performs super crevice corrosion resistance in comparison to the stainless steels. Long lasting clinical usage has showed the perfect biocompatibility of bulk formed-Co alloys (Buckwalter, Einhorn, Simon, 2000).

2.2.2 Oxide of Co-Cr-Mo Alloy

Surface oxide film of a Co-Cr-Mo alloy is characterized as containing oxides of cobalt and chromium without molybdenum (Smith, Pilliar, Metson & Mclntyre, 1991). On the other hand, surface oxide film on another Co-Cr-Mo alloy polished mechanically in de-ionized water consists of oxide species of cobalt, chromium and molybdenum, and its thickness is about 2.5 nm (Hanawa, Hiromoto, Asami, 2001).

2.3 Ti and Ti-Based Alloys:

Attempt to utilize titanium as an implant material date back to 1930s. It was first used in cat femurs. At that time titanium showed a good biocompatibility such as stainless steel and CoCrMo alloy (Vitallium©). Physical and mechanical properties of titanium for this usage made it an alternative implant material compared to stainless steels and Co alloys (Park, Kim, 2007)

Ti and Ti alloys are very interesting materials in implant surgery because of their high biocompatibility and corrosion resistance. This resistance, which is provided by TiO_2 passive layer on the surface, exceeds that of stainless steel and Co alloys. Uniform corrosion is limited even in salt waters. Crevices, pitting and intergranular corrosion resistance of them are excellent. Clinical experiments proved the high biocompatibility of titanium. Titanium alloys are generally used for orthopedic and dental implants more frequently than commercial pure titanium due to their superior mechanical strength (Hao, Li, Sun, Sui, Yang, 2007). However to improve the bone bonding ability of titanium implants, many attempts have been made to modify the structure, composition and chemistry of the titanium surfaces including deposition of bioactive coatings (Buser, Schenk, Steinemann, Fiorellini, 1991) (Pham, Reuther, Matz, Mueller, 2000).

The most important drawback of titanium alloys is the crack sensitivity of them. Notches and scratches, which create stress concentrations on the surface, decrease the fatigue limit of material. Especially on the surface of total joint components,

which are made of porous titanium, this kind of stress concentrations will occur. Therefore design of these parts should be carried out carefully.

The other drawback of titanium alloys is low hardness value compared to Co alloys. Hardness is a definition of plastic and elastic deformation resistance. Micro-hardness tests showed that the hardness of titanium alloys is 15% less than Co alloys. This kind of titanium alloys should not be used unless surface treatment to increase hardness especially as an artificial joint surface is applied.

The ion release of titanium alloys is also important. Some toxic elements (Al, V, Fe, Cu, and Zn) could be released from the bulk into the host tissues. Clinical tests showed that at femoral head, there is retention of toxic elements which are sourced from untreated surface of titanium alloy such as Ti6Al4V. C and N ion implantation is a kind of solution for this problem by increasing the surface hardness and changing the concentration of surface. Before giving a decision of the kind of titanium alloy for implants; it is very important to choose a non-toxic element including titanium alloy (Niinomi, Nakai, Tsutsum, 2010). Figure 2.7 shows the cyto-toxicity of pure metals. Figure 2.8 shows the biocompatibility and corrosion resistance of some pure metals and metallic biomaterials.

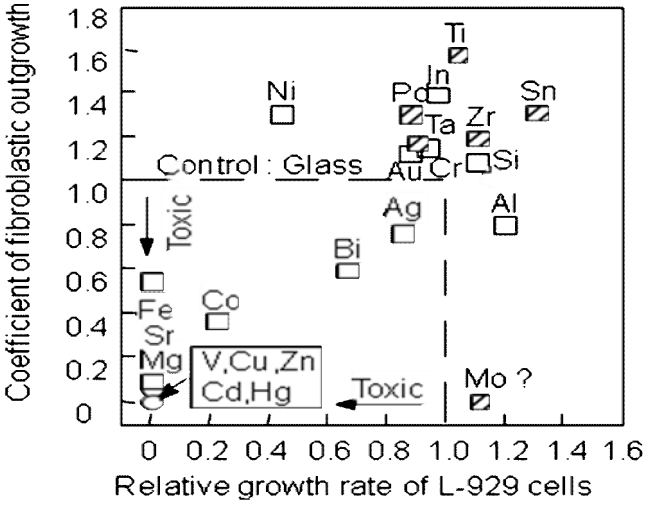

Figure 2.7 Cyto-toxicity of pure metals (Niinomi, Nakai, Tsutsumi, 2010).

Some kind of surface coating techniques (such as micro-arc oxidation) can isolate the surface from releasing of these toxic elements.

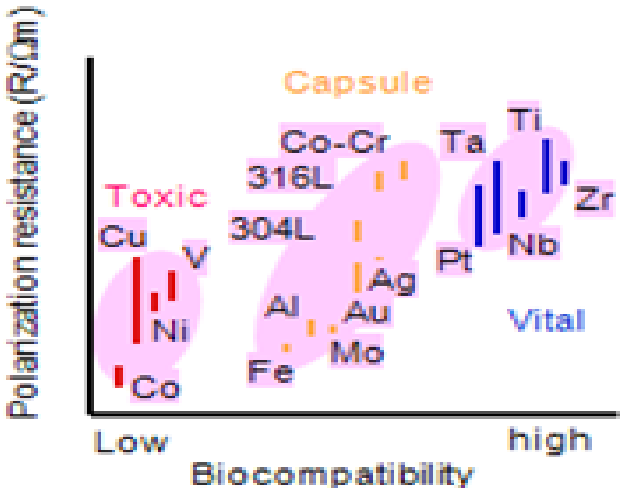

Figure 2.8 Corrosion resistance and biocompatibility of representative pure metals and metallic biomaterials (Niinomi, Nakai, Tsutsumi, 2010)

2.3.1 Types and Properties of Ti and Ti-based Alloys:

One titanium alloy (Ti6Al4V) is widely used to manufacture implants (nearly 60% among titanium alloys). The chemical compositions of pure Ti and Ti alloys are given in Table 2.10-2.12.

Table 2.10 Chemical composition of pure titanium (F67; ASTM, 2000)

Element	Grade 1	Grade 2	Grade3	Grade 4
N	0.03	0.03	0.05	0.05
C	0.10	0.10	0.10	0.10
H	0.015	0.015	0.015	0.015
Fe	0.20	0.30	0.30	0.50
O	0.18	0.25	0.35	0.40
Ti	Balance			

Table 2.11 Chemical Compositions of Ti6Al4V Alloys (ASTM, 2000)

Element	Wrought, forging (F136, F620)	Casting (F1108)	Coating (F1580)
N	0.05	0.05	0.05
C	0.08	0.10	0.08
H	0.012	0.015	0.015
Fe	0.25	0.30	0.30
O	0.13	0.20	0.20
Cu	-	-	0.10
Sn	-	-	0.10
Al	5.5-6.50	5.5-6.75	5.50-6.75
V	3.5-4.5	3.5-4.5	3.50-4.50
Ti	Balance		

Table 2.12 Chemical Compositions of Wrought Ti Alloys (ASTM, 2000)

Element	Wrought Ti8Al7Nb (F1295)	Wrought Ti13Nb13Zr (F1713)	Wrought Ti12Mo6Zr2Fe (F1813)
N	0.05	0.05	0.05
C	0.08	0.08	0.05
H	0.009	0.012	0.020
Fe	0.25	0.25	1.5-2.5
O	0.20	0.15	0.08-0.28
Ta	0.50	-	-
Al	5.5-6.50	-	5.50-6.75
Zr	-	12.5-14.0	5.0-7.0
Nb	6.50-7.50	12.5-14.0	-
Mo	-	-	10.0-13.0
Ti	Balance		

Titanium exists hexagonal close-packed structure (α-Ti) up to 882°C and body-centered cubic structure (β-Ti) above that temperature. The alloying elements change the phases of titanium at room temperature. Effect of element addition to structure of titanium is given in Figure 2.9.

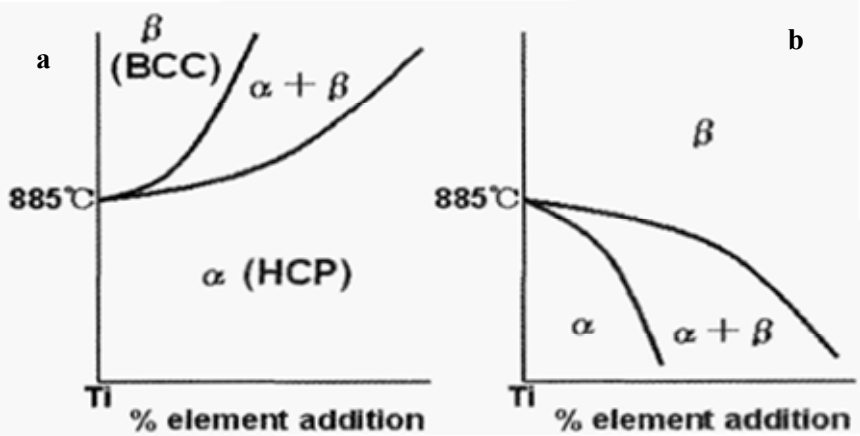

Figure 2.9 Schematic explanation of **Ti-X** two-phase diagram; 885°C is the allotropic transformation temperature.

1-Addition of aluminum stabilizes α phase of titanium by increasing the transformation temperature from α to β phase (Figure 2.9.a).

2- Vanadium stabilizes β phase by lowering the transformation temperature from α to β phase.

α phase of titanium has a good welding capability. High aluminum content increases the strength and high temperature corrosion resistance (300-600°C). These kinds of titanium alloys are not hardened by heat treatment because of single phase. To increase the strength of these alloys, the second or third phase precipitation hardening process is suitable (Park, Kim, 2007). β phase of titanium alloys have low young modulus value with respect to α phase titanium alloys. Therefore these types of titanium alloys are suitable to cope with stress shielding phenomenon among titanium alloys. A part of phase diagram of Ti-Al-V alloy which include 4 w/o V is given in Figure 2.10.

Mechanical properties of some pure Ti and Ti alloys are given in Table 2.13-2.15.

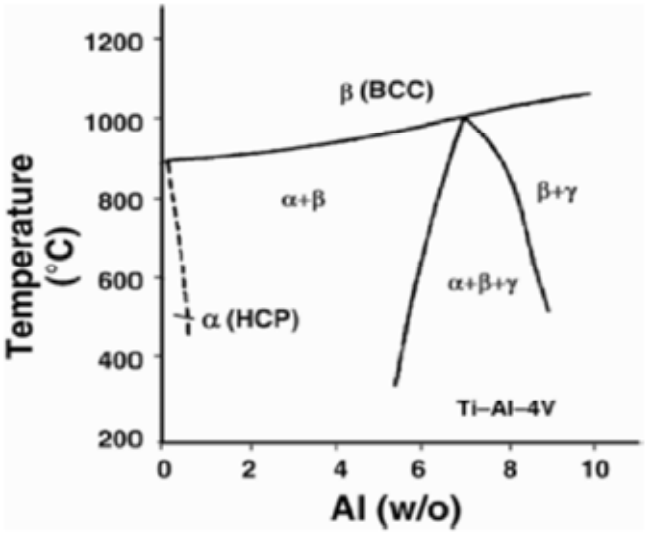

Figure 2.10 Part of phase diagram of Ti-Al-V at 4 w/o V. Reprinted with permission from Smith and Hughes (1966). Copyright© 1966, Institute of Mechanical Engineers (Park, Kim, 2007).

Table 2.13 Mechanical Properties of Pure Titanium (F67, 1992) (ASTM, 2000)

Properties	Grade 1	Grade 2	Grade 3	Grade 4
Tensile strength (MPa)	240	345	450	550
Yield strength (0.2% offset) (MPa)	170	275	380	485
Elongation (%)	24			15
Reduction of area (%)	30	30	25	25

Table 2.14 Mechanical Properties of Ti6Al4V (ASTM, 2000)

Mechanical Property	Metric	Comments
Hardness, Brinell	334	Estimated from Rockwell C.
Hardness, Knoop	363	Estimated from Rockwell C.
Hardness, Rockwell C	36	
Hardness, Vickers	349	Estimated from Rockwell C.
Tensile Strength, Ultimate	950 MPa	
Tensile Strength, Yield	880 MPa	
Elongation at Break	14 %	
Reduction of Area	36 %	
Modulus of Elasticity	113.8 GPa	
Compressive Yield Strength	970 MPa	
Notched Tensile Strength	1450 MPa	K_t (stress concentration factor) = 6.7
Ultimate Bearing Strength	1860 MPa	e/D = 2
Bearing Yield Strength	1480 MPa	e/D = 2
Poisson's Ratio	0.342	
Charpy Impact	17 J	
Fatigue Strength	240 MPa	at 1E+7 cycles. K_t (stress concentration factor) = 3.3
Fracture Toughness	75 MPa.m$^{1/2}$	
Shear Modulus	44 GPa	
Shear Strength	550 MPa	Ultimate shear strength

Table 2.15 Mechanical Properties of Ti Alloys (Robert M. Pilliar, 2009).

Alloys	E (GPa)	Yield strength (MPa)	Tensile strength (MPa)	Elongation (%)	Fatigue strength (10^7)
α-β Alloys					
Ti-6Al-4V	110	860	930	10-15	610-625
Ti-6Al-7Nb	105	795	860	10	500-600
Ti-5Al-2.5Fe	110	820	900	6	580
β / Near - β Alloys					
Ti-12Mo-6Zr-2Fe (TMZF)	74-85	1000-1060	1060-1100	18-22	525
Ti-15Mo-2.8Nb-0.2Si-0.26 (21SR$_X$)	83	945-987	980-1000	16-18	490
Ti-35.5Nb-7.3Zr-5.7Ta (TNZT)	55-66	793	827	20	265
Ti-13Nb-13Zr	79-84	863-908	973-1037	10-16	500

Fatigue strengths of some medical alloys are given in Table 2.16. Figure 2.11 shows the internal structure of Ti-6Al-4V alloy.

Table 2.16 Fatigue strengths (at 10^7 cycles) for some medical alloys

Alloy	Fatigue Strength (MPa)
Ti-6Al-4V (68)	480-590
316L (63)	180-300*
ASTM F-75	310
Grade 3 cP-Ti	330

*annealed and cold worked respectively

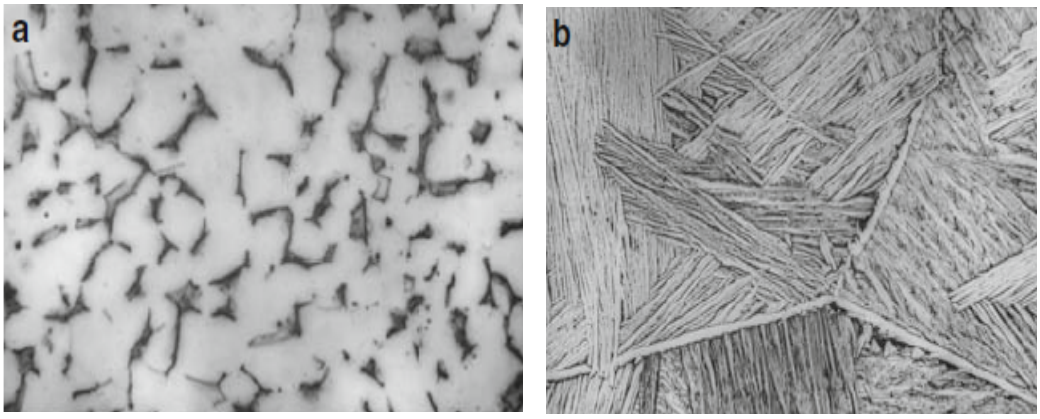

Figure 2.11 Microstructure of Ti-6Al-4V alloy; Microstructure of Ti6Al4V alloy; mill-annealed condition (**a**) – *light regions* are α-phase and *darker zones* are β-phase regions; β-annealed condition (**b**) showing the lighter appearing a-lamellae separated by β-phase lamellae. Note also the domain structures (zones within a single grain with α to β formed on different habit planes, i.e., same α to β orientation relation but involving planes in a different crystallographic orientation) (Robert M. Pilliar, 2009)

2.3.2 Oxide of Titanium Alloys

The film on Ti-6Al-4V alloy was almost the same as that on titanium, containing a small amount of aluminum oxide (Hanawa & Ota, 1991), (Hanawa, 1991). In other words, the surface oxide film on Ti-6Al-4V was a TiO_2 containing small amounts of Al_2O_3 hydroxyl groups, and bound water. Vanadium contained in the alloy was not detected in the oxide film after the alloy was polished.

The Ti-56Ni shape memory alloy was covered by TiO_2-based oxide, with minimal amounts of nickel in both the oxide and metallic states (Hanawa & Ota, 1991),

(Hanawa, 1991). The film on Ti-56Ni was a TiO_2 containing small amounts of metallic nickel, NiO, hydroxyl groups and bound water (Hanawa, 2004).

2.4 Zr-Nb Alloys

Zr is an active element (like titanium) and can form a cohesive and protective oxide ZrO_2 on the surface when it is exposed to oxygen-containing environment. This oxide form is also hard and adequate for wear resistance. Zr-Nb alloys are manufactured in orthopedic devices (femoral hip implant and knee implant components) for compressive loading and resisting wear. Zr-Nb structure has an advantage of resistance for rapid crack initiation and propagation over whole ceramic components such as Al_2O_3, ZrO_2 by reinforcement of oxide layer by Zr-Nb alloy body. Recently these kinds of biomaterials have a great interest among medical devices (Benezra, Mangin, Treska, Spector, 1999).

2.5 Ni-Ti Alloys (Nitinol):

Nitinol is generally used in orthopedic, dental and cardiovascular applications (Haasters, Salis-Salio, Bensmann, 1990). This alloy has shape memory effect and good corrosion resistance (by TiO_2 protective phase on the surface). *In vivo* experiments proved that this alloy is biocompatible although it has high Ni content (Wever, Veldhuizen, Sanders, Schakenrad, 1997), (Kapanen, Ryhanen, Danilov, Tuukkanen, 2001). But this alloy has a concern for long-term usage for toxicity and this drawback limits the usage. Up to date scientific reports showed that corrosion properties of this alloy can be enhanced to the level of 316L stainless steels (Assad, Chernyshov, Jarzem, Leroux, 2003), (Firstov, Vitchev, Kumar, Blanpain, 2002).

Nitinol alloys have shape memory effect. This effect is due to the thermoelastic martensitic transformation (austenite to martensite) by exceeding a critical temperature. It is possible to develop a nitinol alloy whose transformation temperature is close to body temperature. Wires, made of nitinol, are currently used in orthodontics because of its pseudoelastic feature. Nitinol made stents are usually preferred for vascular phenomenon. After insertion of this stents, expansion/deployment property of them is utilized to clear away of a blocked artery.

Human body temperature is nearly 37°C. A nitinol alloy which has a transformation temperature nearly below 37°C is suitable for this aim.

M_S (martensite start) temperature of this alloys are positively related with yield strength of them and fatigue strength of them increases by lowering the M_S temperature. For nitinol, accurate determination of transformation temperature is critical for design and performance in human body (Cisse, Savadogo, Wu, Yahia, 2002).

2.6 Tantalum

It is well known that tantalum is biocompatible via its stable oxide form (Ta_2O_5) on the surface. Porous foam of tantalum is utilized as bone augmentation templates. These foams are made by chemical vapor deposition (CVD) and infiltration of Ta onto vitreous carbon lattice structure. *In vivo* experiments have proved the efficiency of this structure for augmentation purposes. Although the mechanical properties of them are low, they are adequate for bone ingrowths (Zardiackas, Parsell, Dillon, Mitchell, 2001).

2.7 Dental Alloys

In dentistry, metals are used for filling in teeth, fabricating crowns and bridges, partial denture frameworks, orthodontic wires, brackets; and manufacturing dental implants. Requirements for manufacturing dental implants are nearly the same of orthopedic joint replacement implants; they are usually made of commercial titanium or titanium alloys. Orthodontic wires and brackets are made of stainless steels, CoCrNiMo alloys, β titanium and Ni-Ti alloys (because of their low elastic modulus and high strength).

Dental amalgams are formed by addition of Hg to the other amalgam elements. Hg is added to the powder form of amalgam alloy. Powders are produced by lathe cutting Ag-Cu-Sn alloy billets or atomization to give spherical powders. After mixing of these alloys with Hg, partial dissolution occurs and some kind of intermetallic compounds (Ag_3Sn, Ag_2Hg_3, $Sn_{7\text{-}8}Hg$, Cu_3Sn, $Cu_6Sn_{5)}$ are obtained in the structure by depleting whole Hg so this phenomenon hardens the structure by time and it becomes suitable load-bearing filling material for dental applications.

These filling alloys reach to maximum hardness after 24hr. The major advantage of amalgam alloys are their easy in situ formability to a desired shape. Although there are lots of concerns about Hg is not suitable that is a toxic element for body, there is no study to prove this circumstance up to date (Pilliar, 2009).

2.7.1 Dental Casting Alloys

These alloys are usually produced by Au-Based, Co-based, Ni-based and Ti-based alloys. They are used for manufacturing of dental bridges, crowns, inlays, onlays and endodontic posts. Both noble and non-noble metal including alloys can be used for this aim. Chemical composition of dental casting alloys is given in Table 2.17.

Table 2.17 Chemical composition of dental casting alloys (Pilliar, 2009)

Alloy type	**Ag**	**Au**	**Cu**	**Pd**	**Pt**	**Zn**	**Other**	
High noble								
Au-Ag-Pt	11.5	78.1	-	-	9.9	-	Ir (trace)	
Au-Cu-Ag-Pd-*I*	10.0	75.0	10.5	2.4	0.1	1.0	Ru (trace)	
Au-Cu-Ag-Pd-*II*	25.0	56.0	11.8	5.0	0.4	1.7	IR (trace)	
Noble								
Au-Cu-Ag-Pd-*III*	47.0	40.0	7.5	4.0	-	1.5	Ir (trace)	
Au-Ag-Pd-In	38.7	20.0	-	21.0	-	3.8	In 16.5	
Pd-Cu-Ga	-	2.0	10.0	77.0	-	-	Ga 7.0	
Ag-Pd	70.0	-	-	25.0	-	2.0	In 3.0	
Base metal	**Ni**	**Cr**	**Co**	**Ti**	**Mo**	**Al**	**V**	**Other**
Ni-Cr	69-77	11-20	-	-	4-14	0-4	-	Fe, Be, Ga, Mn, B
Co-Cr	-	15-25	44-58	-	0-4	0-2	-	Fe, Ga, Nb, W, B, Ru
Ti	-	-	-	90-100			0-4	

Requirements for these alloys are adequate strength, toughness, wear resistance, corrosion resistance and biocompatibility. For esthetic appearance silicate-based porcelain is bonded to cast metal substrate by porcelain-fused-to-metal (PFM) technique. Before manufacturing of this type of device, thermal expansion coefficient of the coating and substrate should be determined carefully. Thermal expansion coefficient differences of the components are characteristic for the life of composite.

Except in reducing environments, the corrosion process always causes a reaction film to form on metallic materials. Passive film is one such reaction film and is

particularly significant for corrosion protection. When solubility is extremely low and pores are absent, adhesion of film – which is formed in and aqueous solution - to the substrate will be strong. The film then becomes a corrosion-resistant or passive film. Passive film is about 1-5 nm thick and transparent. Due to the tremendously fast rate at which it is formed, passive film readily becomes amorphous. For example, film on a titanium metal substrate was generated in 30 seconds. This was estimated from the time transient of current of titanium at 1V vs. SCE after exposing the metal surface. Since amorphous films hardly contain grain boundary and structural defects, they are corrosion-resistant. However, corrosion resistance decreases with crystallization. Fortunately, passive films contain water molecules that promote and maintain amorphousness (Hanawa, 2004).

2.8 Oxide of Noble Metal Alloys

Au-Cu-Ag alloys and Ag-Pd-Cu-Au alloys for dental restoration are covered by copper oxide and/or silver oxide (Endo, Araki and Ohno, 1989). Dental amalgams (Ag-Sn-Cu-Hg alloys) are covered by tin oxide (Hanawa, Takahashi, Ota, Pinizzotto, 1987). Composition of surface oxide film varies according to environmental changes, though the film is macroscopically stable. Passive surfaces co-exist in close contact with electrolytes, undergoing a continuous process of partial dissolution and r-precipitation from the microscopic viewpoint. In this sense, surface composition is always changing according to the environment. Reconstruction model of surface oxide film on metallic biomaterials is given schematically in Figure 2.12.

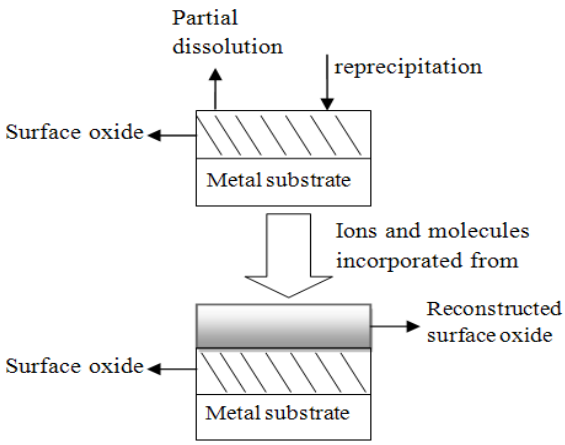

Figure 2.12 Schematic reconstruction model of surface oxide film on metallic biomaterials.

Due to abrasion with bone and other materials, surface oxide film may be scratched and destroyed during insertion and implantation into living tissue. Fretting corrosion also leads to film destruction. Fortunately, surface oxide is immediately regenerated in a biological environment where biofluid surrounds the metallic material. However, the composition and properties of the oxide film regenerated in a biological environment may be different from those in water.

CHAPTER THREE

BEHAVIOUR OF METALLIC IMPLANTS IN SIMULATED BODY FLUID

3.1 Titanium in Simulated Body Fluid

When titanium which has been surgical implanted into the human jaw is characterized using auger electron spectroscopy (AES), its surface oxide film reveals constituents of calcium, phosphorus and sulfur (Sundgren, Bodo, Lundstrom, 1986), (Espostito, Lausmaa, Hirsch, Thomsen, 1999). By immersing titanium and its alloys in Hank's solution and other solutions (Hanawa & Ota, 1991), (Hanawa, 1991), (Hanawa, Okuno, Hamanaka, 1992), (Hanawa, Ota, 1992), preferential absorption of phosphate ions occurs leading to formation of calcium phosphate on their surface (Healy, Ducheyne, 1992).

Hank's solution, whose pH is 7.4, is an artificial biofluid. Its inorganic composition is similar to extracellular fluid. Hydrated phosphate ions are absorbed by a hydrated titanium oxide surface during the release of protons (Hanawa, Ota, 1992). Calcium ions are then absorbed by phosphate ions –which are absorbed on the titanium surface, thus leading to calcium phosphate being formed eventually. On the same note, when titanium is immersed in Hank's solutions containing albumin, a non-uniform and porous albumin-containing apatite is formed (Serro, Fernandes, Saramago, Lima, 1997). The above phenomena are characteristic of titanium and its alloys (Hanawa, 1991).

The surface oxide film regenerated in Hank's solution contains phosphate ions in the outermost layer. Phosphate ions are preferentially taken up during regeneration of surface oxide film on titanium. The resultant film comprises titanium oxide and titanium oxyhydroxide and the latter contains titanium phosphate. Following regeneration, calcium and phosphate ions are absorbed to the film, thus forming calcium phosphate or calcium titanium phosphate on the outermost surface.

Calcium phosphate precipitates faster on a surface film regenerated in a biological system than that in water because seeds of calcium phosphate already exist on the regenerated film. Extrapolating from here, it can be assumed that bone formation is

faster on titanium implanted in hard tissue simply because the surface oxide film is titanium oxide. On this basis, surface modification was attempted on titanium using this repassivation reaction (Hanawa, Hiromoto, Asami, Ukai, 2002). Calcium phosphate is also formed on Ti-6Al-4V and Ti-56Ni alloys after immersion in Hank's solution, but the [Ca]/[P] ratios are smaller than that in titanium (Hanawa & Ota, 1991), (Hanawa,1991). Table 3.1 gives the XPS results of Ti-6Al-4V alloy surface after 300 s immersing of water and Hank's solution.

Table 3.1 XPS results for relative concentrations of elements in surface oxide film on Ti-6Al-4V regenerated in water and in Hank's solution during 300 s immersion (Ishizawa, Ogino, 1995).

Abraded in	**Relative concentrations (at %)**					
	Ti	**Al**	**V**	**O**	**Ca**	**P**
Water	24.5 (0.9)	3.8 (1.1)	0.0 (0.0)	71.8 (0.1)	0.0 (0.0)	0.0 (0.0)
Hanks	21.4 (0.1)	3.2 (0.2)	0.0 (0.0)	73.2 (0.3)	0.1 (0.0)	2.2 (0.0)

3.2 Stainless Steel in Simulated Body Fluid

In pins and wires made from 316L austenitic stainless steel, calcium and phosphorus are present in the surface oxide (Sundgren, Bodo, Lunstrom, Berggren, 1985). The corrosion product of 316L steel implanted in the femur –as part of an artificial hip joint – consists of chromium combined with sulfur, and/or iron combined with phosphorus (where the latter contains calcium and chlorine) (Walczak, Shahgaldi, Heatley, 1998).

For 316L steel polished in de-ionized water, the surface oxide film consisted of iron and chromium oxides which contained small amount of nickel, molybdenum and manganese oxide. The surface oxide also contained a large amount of OH^-.

For specimens immersed in Hank's solution and in cell culture medium, as well as incubated with culture cells, calcium phosphate was formed. Sulfate was absorbed by the surface oxide films and reduced to sulfite in cell culture medium and with the cultured cells. The result in this study suggests that nickel and manganese are depleted in the oxide film. The surface oxide changes into iron and chromium oxides, where a small amount of molybdenum oxide will be present in the human body.

3.3 Co-Cr-Mo Alloy in Simulated Body Fluid

In Co-Cr-Mo alloy, cobalt was dissolved during immersion in the Hank's solution and in cell culture medium, as well as during incubation in a cell culture (Hanawa, Hiromoto, Asami, 2001). After dissolution, surface oxide which consists of chromium and molybdenum was more widely distributed in the inner layer than in the outer layer of the oxide film.

CHAPTER FOUR

SURFACE MODIFICATIONS OF METALLIC IMPLANTS

Surface modification is a process that changes a material's surface composition, structure and morphology, leaving the bulk mechanical properties intact. With surface modification, chemical and mechanical durability, as well as tissue compatibility of surface layer could be improved. Surface property is particularly significant for biomaterials, and thus surface modification techniques are particularly useful to biomaterials. Dry-process (using ion beam) and hydro-process (which is performed in aqueous solution) are predominant surface modification techniques. Apatite coating on titanium with plasma spray, titanium nitride coating with sputter deposition, and titanium oxide growth with morphological control by electrolysis are already available for commercial use as shown in Figure 4.1 (Hanawa, 2004).

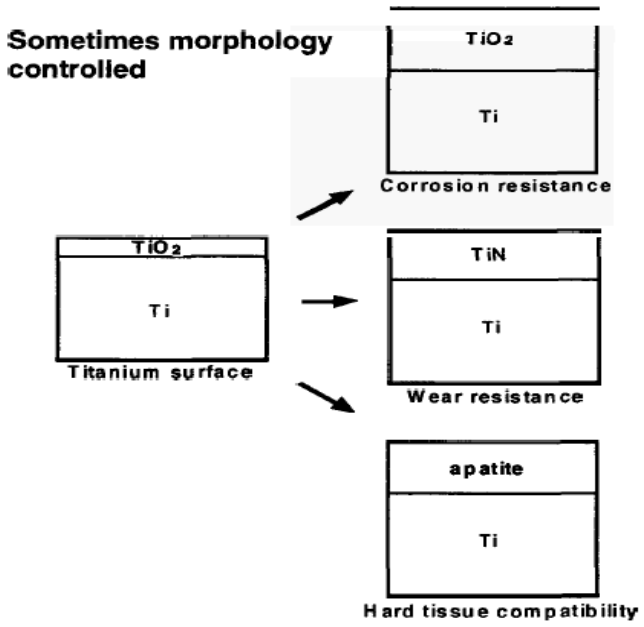

Figure 4.1 Commercial used surface modification techniques of titanium (when it is used as biomaterial)

In biomaterials, chief purpose of surface modification is to improve corrosion resistance, wear resistance, antibacterial property, and tissue compatibility. Figure 4.2 are schematic illustration of artificial hip joint, bone plate and screws.

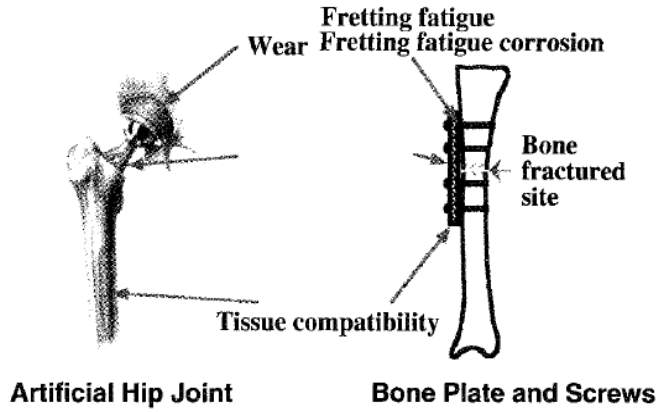

Figure 4.2 Schematic illustrations of artificial hip joint, bone plate and screws, and problems sometimes occurring in clinical use (Hanawa, 2004)

Surface modification processes are categorized into dry processes and hydro-processes. Surface modification techniques being investigated are summarized in Table 4.1 according to their objectives.

Table 4.1 Surface modification techniques for metallic biomaterials (Hanawa, 2004).

Purpose	Techniques	
Improve corrosion resistance	• Immersion • Anodic polarization or electrolysis • Noble metal ion implantation	
Improve wear resistance	• TiN layer deposition • Nitrogen ion implantation	
Improve hard tissue compatibility	Apatite layer Formation	• Immersion • Electrochemical deposition • Plasma Spray • Ion plating • RF magnetron sputtering • Pulse laser deposition
	Non-apatite layer formation	• Immersion in alkaline solution and heating • Immersion in H_2O_2 • Calcium ion implantation • Calcium ion mixing • Hydrothermal treatment • Biomolecule unmobilization
Improve blood compatibility	• Polymer unmobilization • Biomolecule unmobilization	

4.1 Ion Implantation

Ion implantation is an approach for modifying surface properties of materials similar to a coating process, but it does not involve the additional of a layer on the surface. Ion implantation uses highly energetic beam of ions (positively charged atoms) to modify the surface structure and chemistry of materials at low temperature. The process does not adversely affect component dimensions or bulk material properties.

The ion implantation process is conducted in a vacuum chamber at very low pressure (10^{-4} to 10^{-5} torr, or 0.13 to 0.013 Pa). Large numbers of ions (typically 10^{16} to 10^{17} ions/cm^2) bombard and penetrate a surface interacting with the substrate atoms immediately beneath the surface. The interaction of the energetic ions with the material modifies the surface, providing it with significantly different properties than the remainder (bulk) of the material. Specific property changes depend on the selected ion beam treatment parameters, for example, the particular ion species, energy, and total number of ions that impact the surface (Davis, 2004).

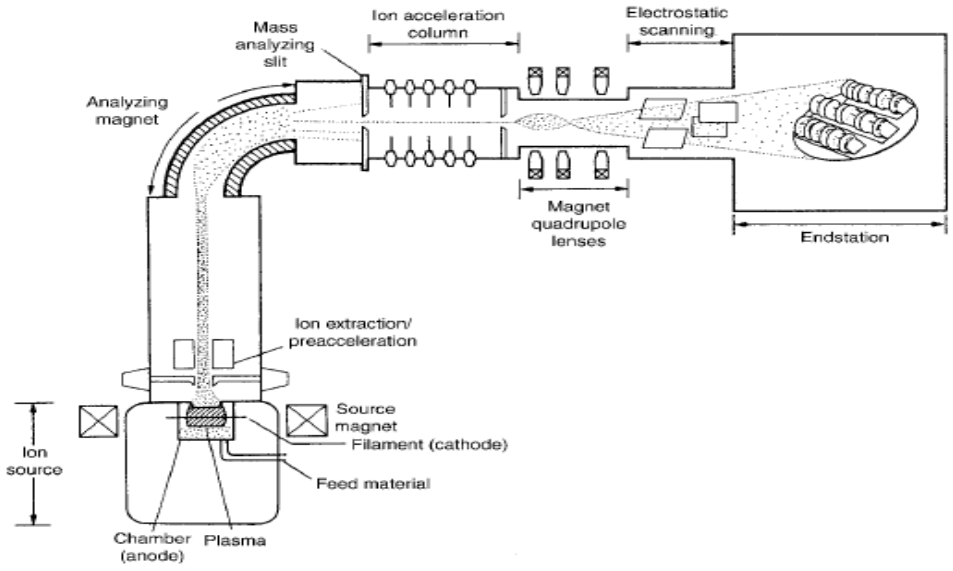

Figure 4.3 Ion implantation system for surface modification of metallic implants. The target in the end station is intended to represent an array of femoral components of artificial knee joints for implantation (Davis, 2004).

Ions are produced via a multistep process in a system such as that shown in Figure 4.3. Ions are initially formed by stripping electrons from source atoms in plasma. The ions are then extracted and pass through a mass-analyzing magnet, which selects only those ions of a desired species, isotope and charge state. The beam of ions is then accelerated using a potential gradient column. Typical ion energies are 10 to 200 keV.

Titanium and cobalt-chromium alloy orthopedic prosthesis for hips and knees are among the most successful commercial applications of ion-implanted components for wear resistance.

4.2 Ion-Beam-Assisted Deposition

Ion-beam-assisted deposition (IBAD) is a thin-film deposition process wherein evaporated atoms produced by physical vapor deposition are simultaneously struck by an independently generated flux of ions (Hubler, Hirvonen, 1994). Material is produced using a high-power electron beam. Components are placed in the vapor, and individual coating atoms or molecules condense and stick on the surface of the component to form the coating. Simultaneously, highly energetic ions (100 to 2000 eV) are produced and directed at the component surface. The component is situated at the intersection of the evaporator and ion beam (Davis, 2004). IBAD process is shown in Figure 4.4.

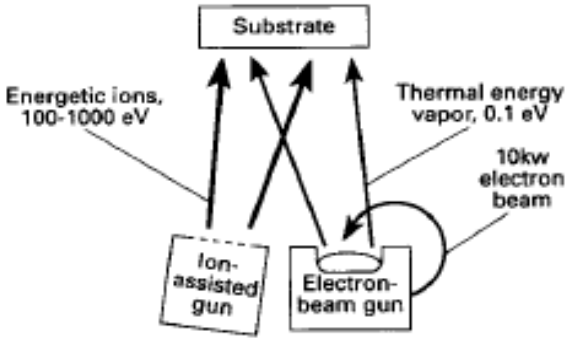

Figure 4.4 Ion-beam-assisted deposition (IBAD) process (Hubler, Hirvonen, 1994).

It significantly improves adhesion and permits control over film properties such as morphology, density, stress level, crystallinity and chemical composition.

The IBAD process is capable of depositing many different types of metallic and ceramic coatings. Samples of metallic coatings include silver, gold, platinum, and titanium. These films are typically used for increasing biocompatibility and providing conductivity or for increasing radiopacity. Silver coatings are also used to create antimicrobial surface on percutaneous and implantable medical devices. Representative ceramic coatings include aluminum oxide, silicon dioxide, titanium nitride and aluminum nitride. These coatings are used for wear-resistant applications.

4.3 Thermal Spray Coatings

Coatings can be applied to the substrates using a variety of processes but commercially the usual route is via a thermal spray process which can take one of several forms – air plasma spraying (APS), vacuum plasma spraying (VPS), high velocity oxyfuel spraying (HVOF) or detonation spraying (DGUN). The first three of these processes involves heating the hydroxyapatite powder in an induced plasma of ionized gases and accelerating the partially melted particles towards a metal substrate where they impact and freeze to form the coating (Grainger, 1989), (Bernecki, 1992). Thermally sprayed coatings have a characteristic layered structure which is illustrated in Figure 4.5. Individual powder particles assume splat shapes on the substrate oriented parallel to the substrate surface producing high levels of anisotropy and leaving isolated pores. The result is a coating with a porosity that varies from 2% to 20%, which contains both amorphous and crystalline phases. Small particles have a tendency to melt rapidly and evaporate. Large particles may only partially melt leaving an amorphous splat with a crystalline core. The original particle size and morphology, the plasma gas mixture, working distance, dwell time of the particles, and substrate temperature will all influence the final structure of the ceramic coating.

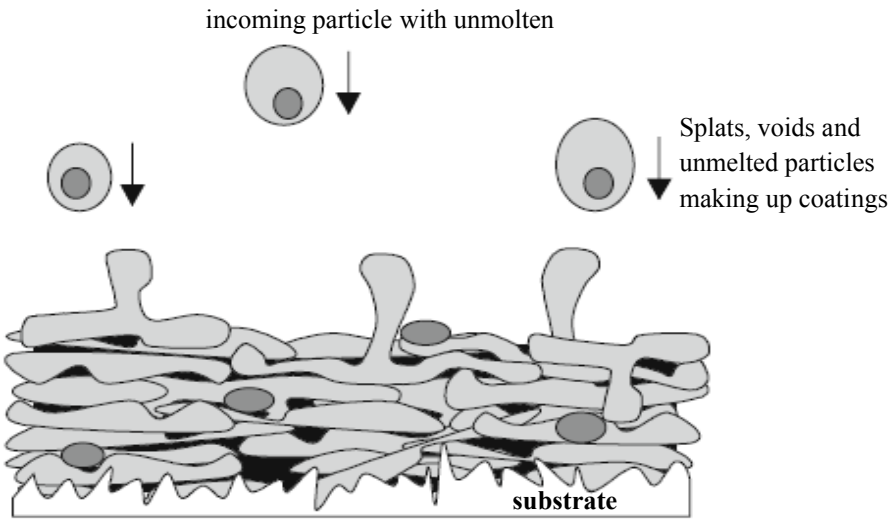

Figure 4.5 Schematic diagram showing a cross-section through a thermally sprayed coating (Turner, 2009)

Vacuum plasma spraying is carried out in an argon atmosphere at a temperature of >10,000 ºC, as illustrated in Figure 4.6. The dwell time is a fraction of a second and the substrate temperature typically 300 ºC. The starting powders for the process are angular with a diameter of approximately 100µ. They have been calcined and crushed. X-ray diffraction analysis shows that they are 80% crystalline in nature prior to spraying. The resultant coatings have a crystallinity of 60%, a porosity of 6%, and are in the order of 40µm in thickness (Gledhill, Turner, Doyle, 1999). By way of contrast, DGUN spraying is carried out in an oxygen and acetylene atmosphere; it involves an explosive spark discharge at temperatures in excess of 3,000 ◦C and particle speeds of 600 m/s. The coatings produced have a high density and superior adherence to the substrate.

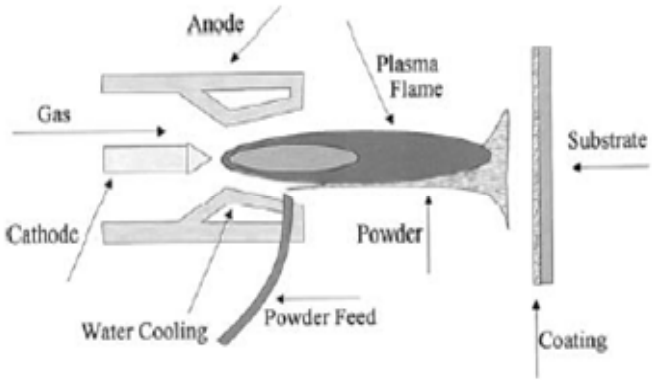

Figure 4.6 Schematic diagram showing the vacuum plasma spraying technique (Turner, 2009).

The biological performance of the coating system will depend on a number of factors – the size and distribution of the porosity, micro crack formation, residual stresses, the oxide content and the amorphous: Crystalline ratio.

4.4 Vapor Deposition Processes

Vapor deposition processes can principally be divided into two types:

• Physical vapor deposition (PVD) processes, which require creation of material vapors (via evaporation, sputtering, or laser ablation) and their subsequent condensation onto a substrate to form the film

• Chemical vapor deposition (CVD) processes, which are generally defined as the deposition of a solid material from the vapor phase onto a (usually) heated substrate as a result of numerous chemical reactions.

In general, CVD processes have the advantage over PVD processes of good throwing power, while PVD processes have higher deposition rates than those in CVD processes (Davis, 2004).

4.4.1 Physical Vapor Deposition

Since it was introduced to the medical device industry in the late 1980s, PVD has become widely used to deposit wear-resistant thin-film coatings on a variety of medical devices, including orthopedic implants, pacemakers, surgical instruments, orthodontic appliances, and dental instruments. The value of PVD technology rests in its ability to modify the surface properties of a device without changing the underlying material properties and biomechanical functionality. In addition to enhanced wear resistance, PVD coatings reduce friction, are compatible with sterilization processes, provide decorative colors, and improve corrosion resistance. The most commonly used coating is TiN, but ZrN, AlTiN, TiAlN, CrN, and amorphous carbon are being tested as alternative biomedical coatings (Davis, 2004). Properties of various PVD coatings are listed in Table 4.2.

Table 4.2 Properties of PVD biomedical coatings (Davis, 2004)

Property	Coatings					
	TiN	**ZrN**	**AlTiN**	**TiAlN**	**CrN**	**Amorphous carbon**
Hardness, HV (a)	2900±200	2800±200	4500±500	2600±400	2500±400	8000
Adhesion, N (b)	70	70	70-80	60	70	80
Oxidation temperature,˚C (˚F)	500 (930)	600 (1110)	800(1470)	800(1470)	700 (1290)	500 (930)
Coefficient of friction (c)	0.65	0.61	0.42	1.70	0.55	0.10
Surface roughness (d) (R_a), µm	0.2	0.2	0.4	0.4	0.2	0.02
Ductility (e), %	1.19	1.01	1.2-1.5	1.2-1.5	…	…
Color	Gold	Gold	Black	Bronze	Silver	Black
(a) Vickers hardness test at 50 g load. (b) Critical normal force in newton required to detach the coating from the substrate. (c) Measured between 100Cr6 ball and coated substrate. (d) Measured by Dektak surface profilometer in micrometers. (e) Done by acoustic four-point bend test. Amount of deformation before cracking. Source: IonBond						

4.4.2 Chemical Vapor Deposition

In this process, the substrate is placed inside a reactor to which a number of gases are supplied. The fundamental principle of the process is that a chemical reaction takes place between the source gases. The product of that reaction is a solid material with condenses on all surfaces inside the reactor. Principle of CVC process is given in Figure 4.7.

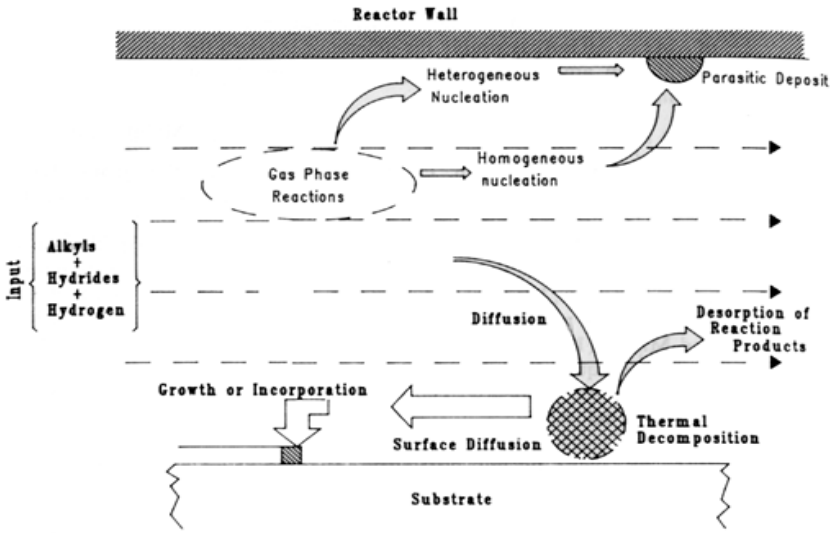

Figure 4.7 Principle of Chemical Vapor Deposition Process (Moon, Houng, 1993)

Diamondlike carbon (DLC) films are hard (up to 80 GPa, or 12 psi × 106) amorphous films produced by CVD, plasma-assisted CVD (PACVD), ion-beam processing, IBAD, and ion plating (Kihara, Watanabe, Abe, 1984). Because the biocompatibility of DLC is excellent, these films are being considered as coatings for metallic implants to improve their compatibility with body tissues. Tissue can adhere well to carbon implants and sustain a durable interface. Also, in the presence of blood, a protein layer is formed that prevents the formation of blood clots at the carbon surface. Carbon-fiber implants can promote the rapid ingrowth of tissue and are used successfully for ligament repair. Another potential application for DLC is coatings for coronary stents. Studies have shown that DLC-coated stainless steel stents implanted in pigs resulted in decreased thrombogenicity and neointimal hyperplasia (Hobo, Iwata, 1985).

4.5 Micro Arc Oxidation

Recently, low adherence of coatings to the substrates remains to be a main problem faced in practice. Among the methods used to obtain good adhesion properties, the micro arc oxidation (MAO) method has gained much interest, because both the roughness and chemical composition of the coating layer can be controlled by the MAO conditions (substrate, temperature, current, voltage, electrolyte) (Ishizawa, Ogino, 1995), (Yerokhin, Nie, Leyland, Matthews, 1999). In addition this method used to produce the oxide layer on the surface. Because the biocompatibility of Ti is closely related to the properties of the surface oxide layer. Compared with films made by traditional anodic oxide methods, the film by MAO is much thicker and harder and attaches to the substrate more firmly (Wang, Dong, Chen, Lei, 2005). Also it has been reported that ceramic film prepared with MAO on a Ti alloy surface attaches firmly to the substrate and is bioactive, which indicates a good prospect for *in vivo* tests (Zhang, Han, Huang, Sun, 2004).

During the MAO process, charged ions of the electrolytes will enter the ceramic film by diffusion and electrophoresis and thus imposes on the film compositions and properties combining both substrates and electrolytes (Groot, Klein, Wolke, Blieck-Hogervorst, 1990).

By applying a positive voltage to a Ti specimen immersed in an electrolyte, anodic oxidation (or anodizing) of Ti occurs to form a TiO_2 layer on the surface. When the applied voltage is increased to a certain point, micro-arc occurs as a result of the dielectric breakdown of the TiO_2 layer. At the moment that the dielectric breakdown occurs, Ti ions in the implant and OH^- ions in the electrolyte move in opposite directions very quickly to form TiO_2 again (Shirkhanzadeh, 1995). The newly formed TiO_2 layer, which is beneficial for the biological performance of the implants, is both porous and firmly adherent to the substrate. Another advantage of this MAO process is the possibility of incorporating Ca and P ions into the surface layer by controlling the composition and concentration of the electrolyte (Ishizawa, Ogino, 1995), (Yerokhin, Nie, Leyland, Matthews, 1999). The presence of Ca and P ions in the porous TiO_2 coating layer can further enhance the bonding between the implants and the bone with anchorage (Nie, Leyland, Song, Yerokhin, 1999), (Voevodin, Yerokhin, Lyubimov, Donley, 1996), (Zhao, Yang, Han, 2006). Figure 4.8 shows the dielectric breakdown when micro arc occurs.

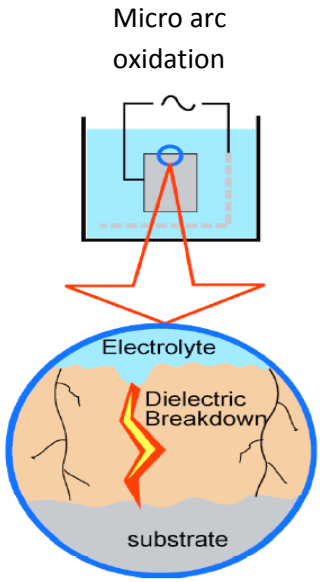

Figure 4.8 Dielectric breakdowns during MAO process

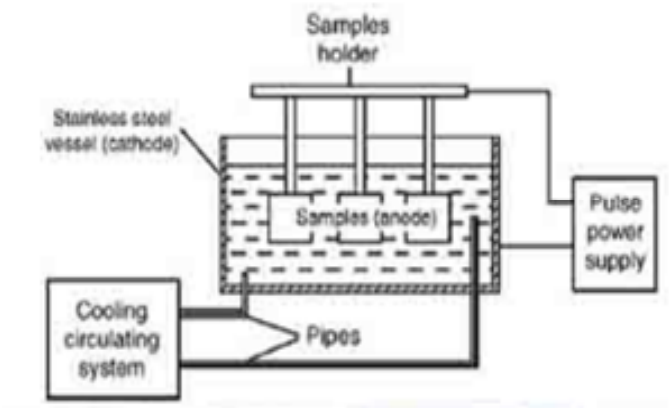

Figure 4.9 Micro Arc Oxidation Process

Micro arc oxidation process scheme and setup are given in Figure 4.9-4.10. MAO parameters of some researchers are given in Table 4.3.

Figure 4.10 Micro Arc Oxidation System (Plasma Technology, 2011)

Table 4.3 MAO parameters of some researches

Article	Process	Voltage	Current	Electrolyte		Duration
(Nie, Leyland, Matthews, 2000)	MAO (Micro arc oxidation) + Electrophoretic deposition	400-450V	20-40 mA/cm^2	Phosphate salts including solution (MAO) HAP solution (Electrophoretic deposition)		5-10 min.
(Filho, Lidizio, Sera, Damascno, 2006)	MAO	140V	-	0.3 M calcium acetate 6 M sodium bicarbonate		3 min.
		110V	-	0.3 M calcium acetate 0.1 M sodium monohidrogen phosphate		10 min.
(Shi, Wang Q., Wang F., Ge, 2009)	MAO	-	-	Calcium glycerophosphate, 0.2 M 0.04 M 0.06 M 0.08 M	Calcium acetate monohydrate 0.1 M 0.2 M 0.3 M 0.4 M	10 min.
(Kim, Ryu, Sung, 2007)	MAO	320-340V	34-35A	Calcium cloride 0.05 M 0.075 M 0.1 M 0.125 M 0.15 M	Potassium phosphate monobasic 0.05 M 0.05 M 0.05 M 0.05 M 0.05 M	4 min.
(Chen, Shi, Wang, Yan, 2006)	MAO	260-420V	0.5 A/cm^2	0.13M Calcium acetate monohydrate 0.06M sodium biphosphate dihydrate		60 min.
(Liu, Wang, Shimizu, Igarashi, 2005)	MAO + Hydrothermal process	350 V 380 V 350 V 380 V 350 V 380 V 350 V 380 V 350 V 380 V	50 A/cm^2 50 A/cm^2 100 A/cm^2 100 A/cm^2 200 A/cm^2 200 A/cm^2 100 A/cm^2 100 A/cm^2 200 A/cm^2 200 A/cm^2	Calcium glyserophosphate 0.06 M 0.06 M 0.06 M 0.06 M 0.06 M 0.06 M 0.04 M 0.04 M 0.04 M 0.04 M	Calcium acetate 0.25 M 0.25 M 0.25 M 0.25 M 0.25 M 0.25 M 0.20 M 0.20 M 0.20 M 0.20 M	-
(Wang Y., Nan, Chen, Ning, 2006)	MAO + Biyomimetic process in SBF	380-450V	40-90 A/cm^2	25 g/L sodium phosphate		-
(Li, Lee, Cui, Choi, 2008)	MAO + Evaporation with electron beam	270V	-	0.15 M Calcium acetate monohydrate 0.02 M Calcium glyserophosphate		3 min.
(Han, Hong, Xu, 2002)	MAO + Hydrothermal process	300V	-	0.2 M Calcium acetate monohydrate		1min.

CHAPTER FIVE

EXPERIMENTAL STUDIES

5.1 Importance of Magnesium for the Study

Mg is one of the elements which take place of calcium in biologically apatite. The lack of magnesium causes problems in every step of skeletal metabolism. Some of these problems are the reduction of bone growth, osteoblastic and osteoclastic activities, osteopenia and bone brittleness (Percival, 1999). It's known that; tooth enamel, dentine and bone include Mg in order of 0.44, 1.23 and 0.72% in weight (LeGeros, 1991). In view of the ongoing discussion, Mg or MgO rich porous oxide layer obtained by MAO is expected to increase the bioactivity of Ti6Al4V. It is well known that MgO is stable only at pH above 12, thus pH of MAO bath has increased to 12 by NaOH addition.

5.2 Scope of the Work

Scope of the study is to obtain a composite oxide which is porous, well-adherent and integrated with elemental or oxide form of Mg inside TiO_2 on the surface of Ti alloy. The pores, which can be modified by MAO to improve bioactivity, can be embedded with a ceramic oxide structures which include CaP compounds. It is expected that elemental or oxide form of Mg integrated with oxide film, can develop a better biocompatibility (Bilgi, Forsti, Gregoriani, Ripamonti, 1992).

Our aim was to deposit bioactive TiO_2 ceramic film impregnated with Mg ion, in elemental or oxide form, with an anticipation of high corrosion resistance, and high bone forming ability on a substrate in order to develop a biocompatible surface.

Electrochemical characterization, in parallel to other characterization studies, of this surface has been carried out using potentiostat/galvanostat in saline solution.

5.3 Sample Preparation

In experimental studies 2 cm^2 surface areas of Ti6Al4V samples were used as substrate. Samples are grinded by 80x, 240x, 400x, 800x, 1000x, 1200x, 2000x SiC

sandpaper and polished by diamond colloidal suspension. After that, ultrasonic cleaning was carried out in distilled water and ethanol solution. Figure 5.1 shows the drawing of the sample which was used in experiments.

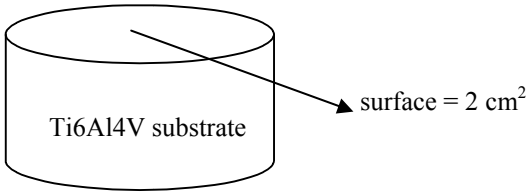

Figure 5.1 Sample which is used in experiments

5.4 Preparation of Electrolytes

Totally 4 electrolytes were used in experiments. Electrolytes were prepared using distilled water into which predetermined chemicals were added while using magnetic stirrer. Electrolyte No.1 was prepared for pre-coating the samples with $Mg(OH)_2$ prior to MAO processing. Electrolyte No.2 and No.3 with different amount of magnesium content was prepared for MAO processing to incorporate Mg in TiO_2. Also another electrolyte, which does not include Mg, was prepared to compare with other electrolytes. Chemical composition and properties of the electrolytes are given in Table 5.1.

Table 5.1 Composition and properties of electrolytes used in this study.

Chemical content and solution properties	**Electrochemical deposition of $Mg(OH)_2$**	**Micro Arc Oxidation**		
		Without Mg	**With Mg**	
	Electrolyte No.1	**For comparison purposes**	**Electrolyte No.2**	**Electrolyte No.3**
Magnesium chloride	0.25 M	-	-	-
Magnesium nitrate	0.25 M	-	-	-
Calcium acetate hydrate	-	0.0564 M	0.0564 M	-
Calcium glycerophosphate hydrate	-	0.0068 M	0.0068 M	0.0068 M
Magnesium acetate tetrahydrate	-	-	0.0282 M	0.0282 M
pH	8.8	12	12	12
Electrical conductivity	67.9 mS/cm	12.6 mS/cm	12.25 mS/cm	8.5 mS/cm

5.5 Electrochemical Deposition of $Mg(OH)_2$

Micro arc oxidation was carried out on Ti6Al4V samples either as pre-coated with $Mg(OH)_2$ or as received. Surface of the samples was mechanically polished as described before. Samples were kept in desiccator until the test was carried out.

Electrochemical coating process was carried out using potentiostat/galvanostat in galvanostatic mode. Coating parameter is given in Table 5.2.

Table 5.2 Process parameters for galvanostatic coating.

Counter Electrode	Graphite
Working Electrode	Ti6Al4V
Reference Electrode	Saturated calomel electrode
Current	-5 mA
Time	1 hour
Electrolyte	0.25 M $MgCl_2$ 0.25 M $Mg(NO_3)_2$
pH	8.8
Conductivity	67.9 mS/cm
Temperature	Room temperature

After coating procedure, surface of the samples were dried by hot air and kept in desiccators for characterization studies.

5.6 MAO Coating

MAO coatings have been carried out using Keronite KT-G2 power supply. Process parameters for MAO experiments are given in Table 5.3. For the process parameters, current and lapse of time in particular, to be determined, couple of free runs were experienced. As a result the exact test condition was reached as given in Table 5.3. Tests were conducted in duplicate form at pre-determined test conditions and results were given as an average of the two. pH of each electrolytes were buffered at 12 by adding NaOH into the test solution. Tests were run at three pre-determined constant current. The timing for the process was determined by the formation of an intense sparking at the applied current, thus the experiment was terminated soon after the state of intense sparking has reached. During MAO

process, change in voltage and current were recorded as a function of time in ten second intervals. After coating process of the samples, temperatures of the electrolytes were measured nearly 30º C. Following the coating process samples were cleaned by distilled water and dried with hot air before stored in desiccator for further characterization studies.

Table 5.3 Process parameters of MAO experiments.

Electrolyte without Mg		**Electrolyte No. 2**		**Electrolyte No. 3**	
Experiment 1	Current= 0.5 A Time= 5 min.	**Experiment 5**	Current= 0.5 A Time= 5 min.	**Experiment 9**	Current= 0.5 A Time= 5 min.
Experiment 2	Current= 1 A Time= 3 min.	**Experiment 6**	Current= 1 A Time= 3 min.	**Experiment 10**	Current= 1 A Time= 3 min.
Experiment 3	Current= 2 A Time= 2 min.	**Experiment 7**	Current= 2 A Time= 2 min.	**Experiment 11**	Current= 2 A Time= 2 min.
Experiment 4 **(MgO pre-coated)**	Current= 1 A Time= 3 min.	**Experiment 8** **(MgO pre-coated)**	Current= 1 A Time= 3 min.	**Experiment 12** **(MgO pre-coated)**	Current= 1 A Time= 3 min.

5.7 Corrosion Tests

Parameters of Tafel scan are given Table 5.4. Corrosion tests of samples were carried out using saline solution (0.9% NaCl in distilled water, pH=6.8). In this electrolyte, open circuit potential (OCP) of test samples was measured for 60 minutes and then Tafel extrapolation was obtained by scanning the electrode potential between ± 30 mV with respect to OCP at a rate of 0,17 mV. Tafel extrapolation was carried out using a three electrode cell where calomel and graphite was used as reference and working electrode respectively.

Table 5.4 Tafel scan parameter of corrosion tests.

Initial E (V)	-0.03
Final E (V)	0.03
Scan rate (mV/s)	0.17
Tafel potentials	Versus open circuit potential

Anodic and cathodic parts of Tafel scanning were used to calculate i_{corr}, $ß_a$ and $ß_c$ by using Gamry Echem Analyst. Then they were used to obtain polarization resistance (R_p) of the samples to compare the corrosion behaviors of the surfaces.

5.8 Characterization Methods

5.8.1 Scanning Electron Microscopy

As shown in Figure 5.2, morphological and chemical analyses of coatings were determined by EDS system attached to scanning electron microscope with 20 kV acceleration voltage. Spot size of EDS was 45 nm. Surface area of coatings is 2 cm^2.

Figure 5.2 Scanning electron microscopy (Jeol JSM-6060) coupled with EDS system.

5.8.2 X-Ray Diffractometer

Phase analyses of coatings were determined by X-Ray diffractometry shown in Figure 5.3. Analyses were carried out by 36 mA current, 40 kV potential of CuK_α radiation with 4 degree/min scanning rate.

Figure 5.3 X-Ray Diffractometry (Rigaku D/max-2200/PC)

5.8.3 Surface Profilometry

Surface roughnesses of coatings were analyzed by XP2 surface profilometry shown in Figure 5.4. Analyses were carried out by 0.5 mm/s scan rate, 5 mm scan size and 0.25 mm cut off length by gaussion filter.

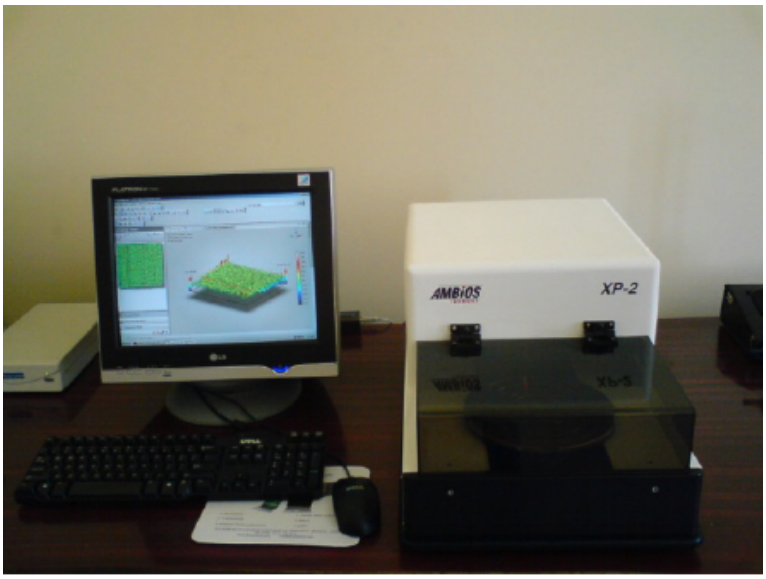

Figure 5.4 Surface Profilometry (Ambios XP2 Stylus Profiler).

5.8.4 Optical Micrographs

Optical images of the surfaces were analyzed by Nikon-Eclipse ME600D optical microscope shown in Figure 5.5. Surfaces were analyzed by using Nikon DS-Fi1 camera and NIS-elements D 2.30 image analyses program.

Figure 5.5 Optical Microscope

CHAPTER SIX

RESULTS AND DISCUSSIONS

6.1 Electrochemical Coating of $Mg(OH)_2$

Electrochemical deposition of $Mg(OH)_2$ was carried out galvanostaticaly at a current density of -5mA. Prior to the deposition, open circuit potential of the sample, was recorded for 60 minutes before the electrochemical deposition as given in Figure 6.1. Change in potential during the galvanostatic deposition was recorded and an example is given in Figure 6.2.

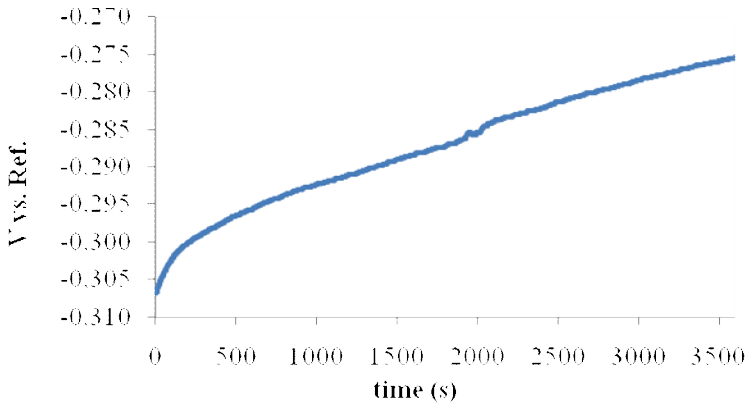

Figure 6.1 Open circuit potential variation of samples before galvanostatic coating

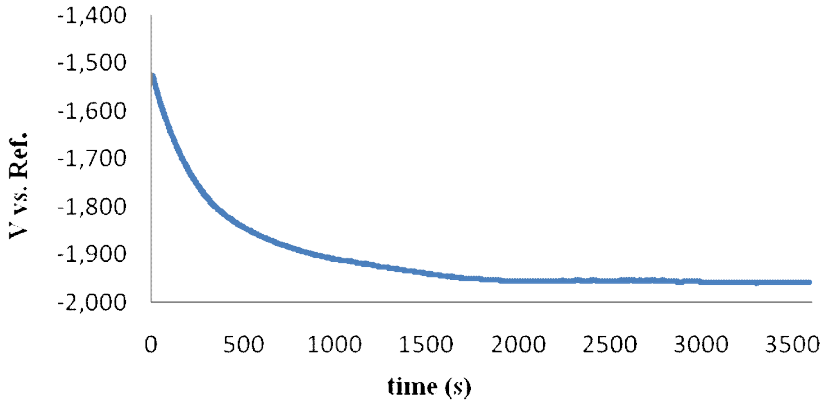

Figure 6.2 Potential change during galvanostatic coating at -5 mA/cm^2

As shown in Figure 6.1, open circuit potential has gradually increased in time. Titanium alloys have a tendency to passivate in the presence of oxygen. According to

this figure, increase in open circuit potential indicates that the more Ti6Al4V stays in the electrolyte, the more it becomes passivated reaching to a more stable state.

Decrease in electrode potential of test sample with respect to time during galvanoststic deposition means that the surface of titanium becomes gradually activated by the formation of surface film densely populated with cracks as shown in Figure 6.3.

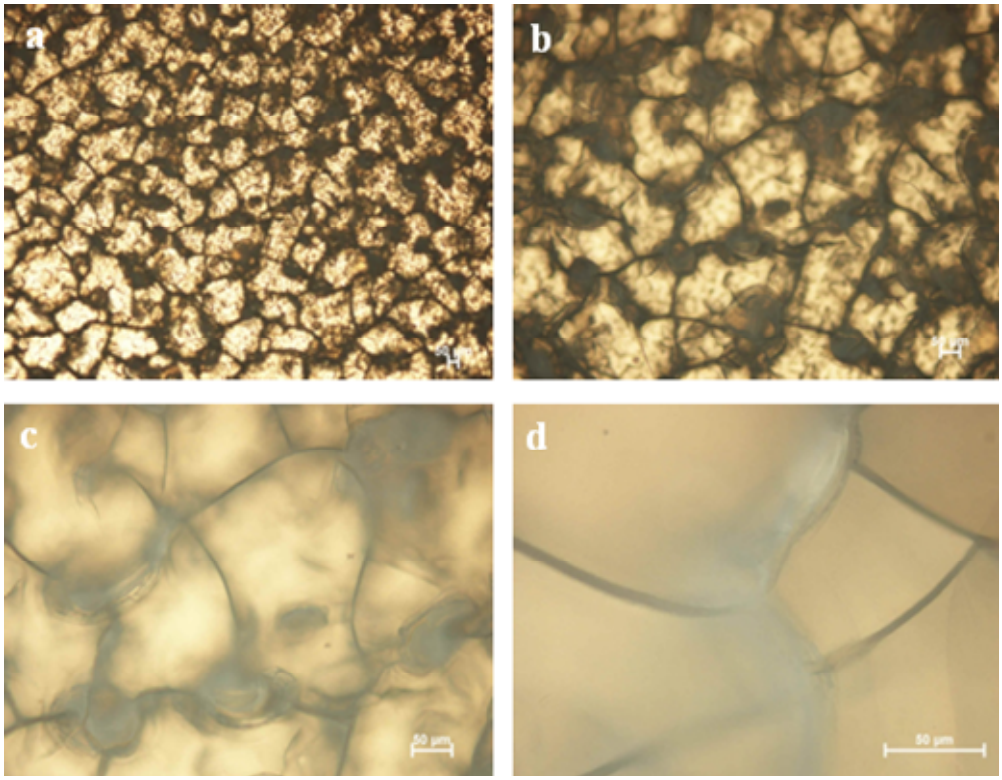

Figure 6.3 a)5x, b)10x, c)20x, d)50x magnification. Cracks on the surface of Ti6Al4V after galvanostatic deposition.

Scanning electron microscopy images of the cracks are given in Figure 6.4. Forms and size of the cracks on the surface are well indicated. It is expected that the crack sizes and density increases with increasing time of depositon, since residual stresses increases with increasing film thickness. A morfological change in film was obserwed at and around crack sites. This was postulated to occure due to the increasing current density at these sites which promoted the formation of a much finer crystals.

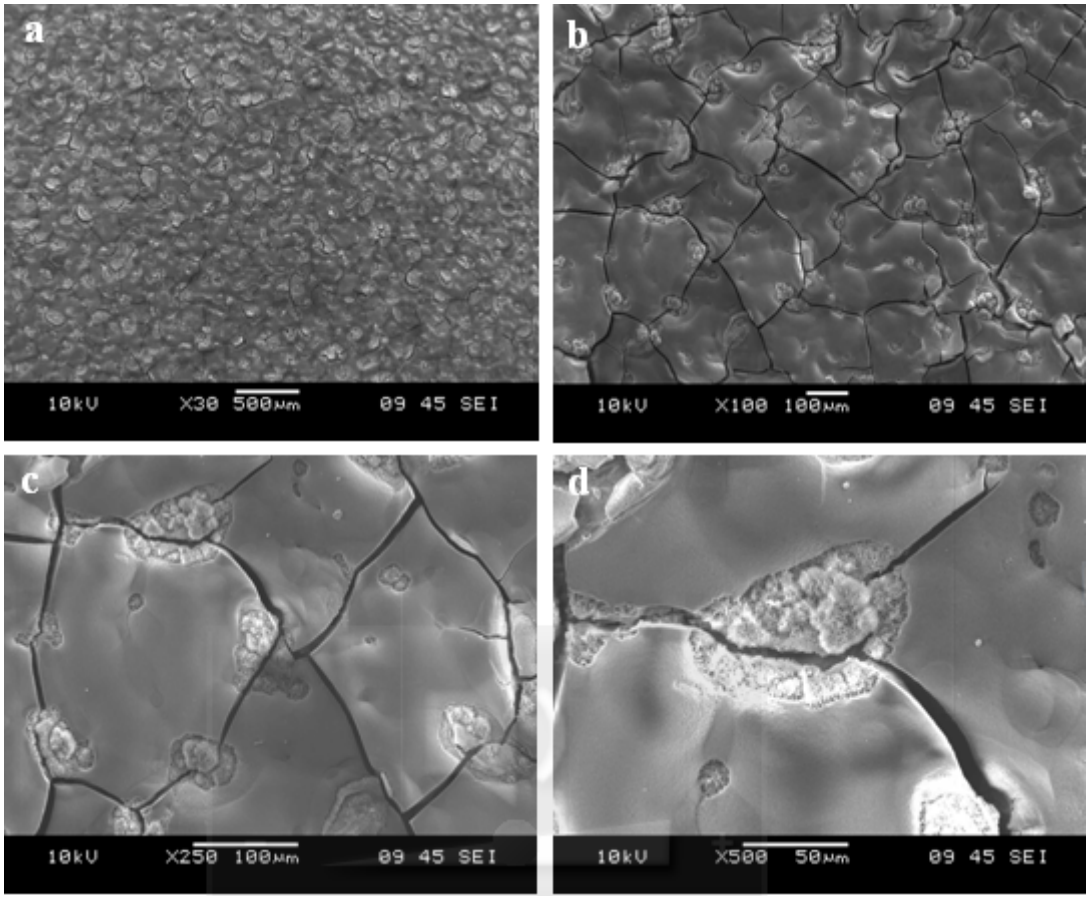

Figure 6.4 SEM images of the cracks after galvanostatic deposition. a)30x, b)100x, c)250x, d)500x magnification .

6.2 Micro Arc Oxidation

Potential variations during micro arc oxidation process are given in Figures 6.5, 6.6 and 6.7.

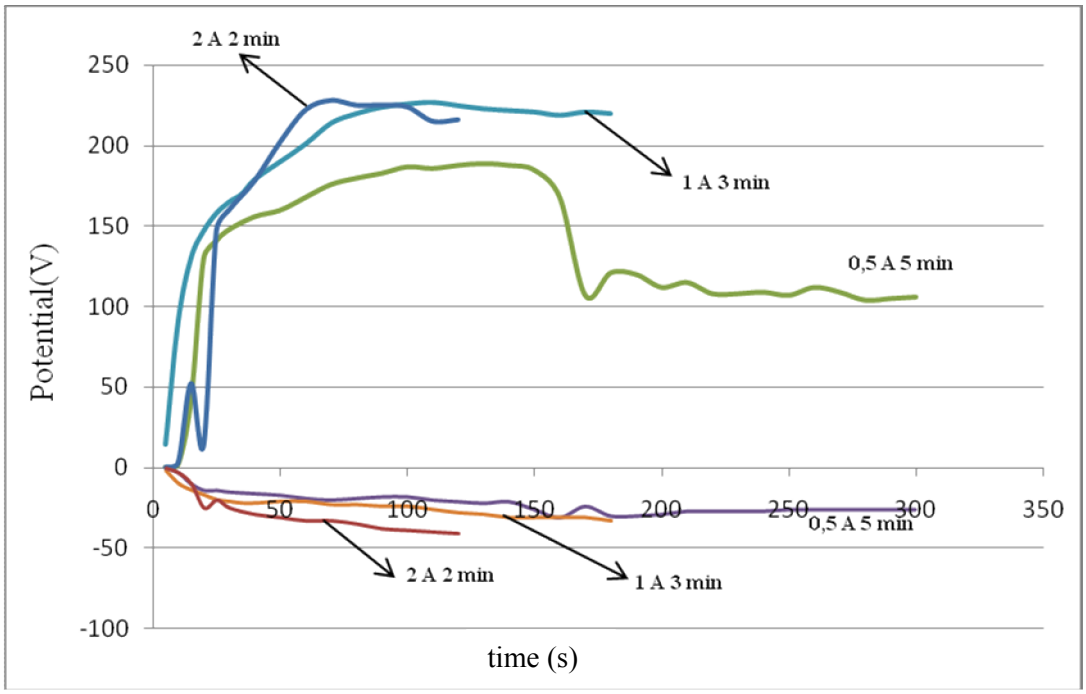

Figure 6.5 Potential variations in electrolyte No.2 measured at different currents applied for the time intervals as indicated on curves.

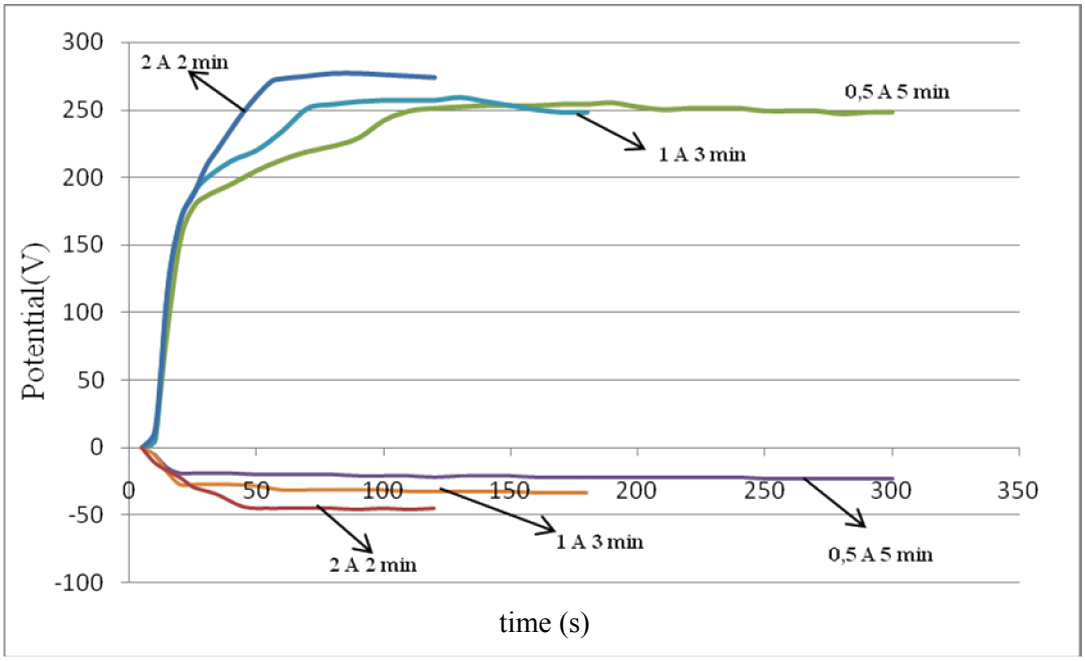

Figure 6.6 Potential variations in electrolyte No.3 measured at different currents applied for time intervals as indicated.

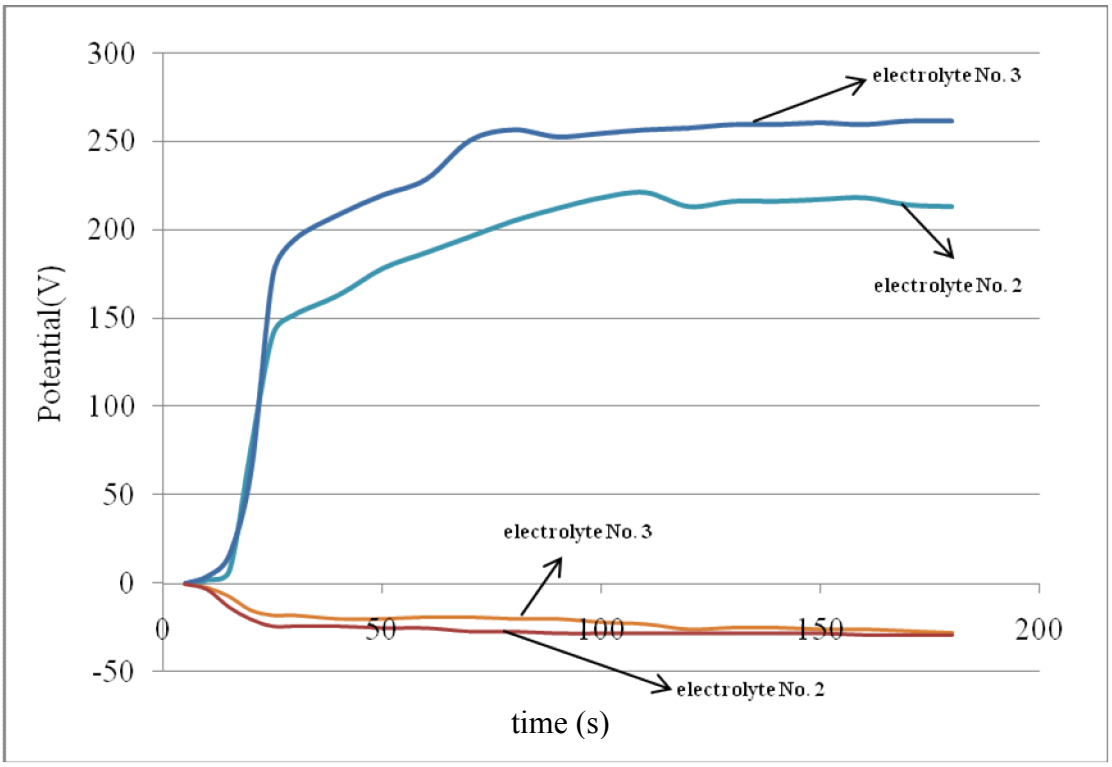

Figure 6.7 Potential variations of MgO coated samples as a function of time during MAO process run at 1 Amps for 3 minutes in electrolyte No.2 and No. 3.

6.3 SEM Images of MAO Coated Surfaces

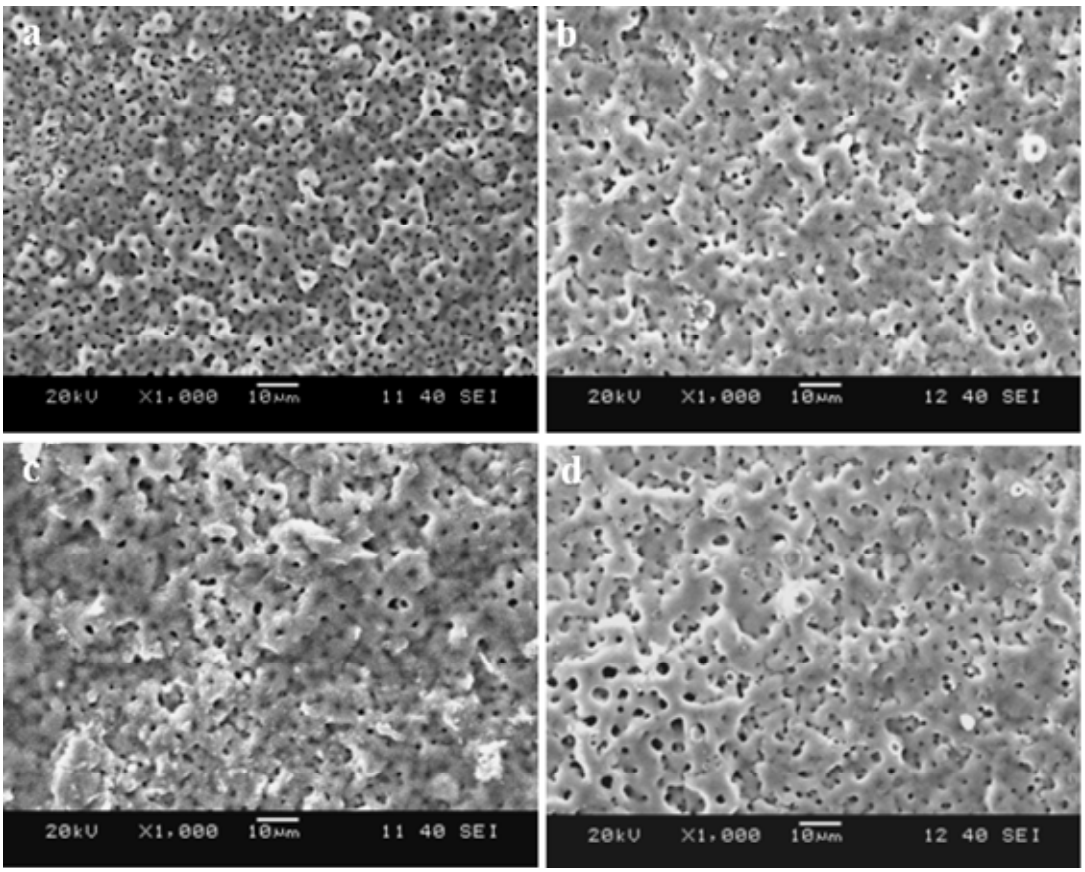

Figure 6.8 SEM image of samples treated in electrolyte No. 2. a) 0.5 A, 5 min. b) 1 A; 3 min. c) 2 A, 2 min. d) 1 A, 3 min. pre- coated with MgO

In the electrolyte No. 2, by increasing current, porosity of the surface has changed and decreased as shown in Figures 6.8a, b and c. Homogenous structure obtained at low current has changed into heterogeneous ones in the same order. Surface roughness also found to increase with increasing current form 0.5 to 2 Amps. MgO pre-coating process has not created any differences in morphology for the electrolyte No. 2.

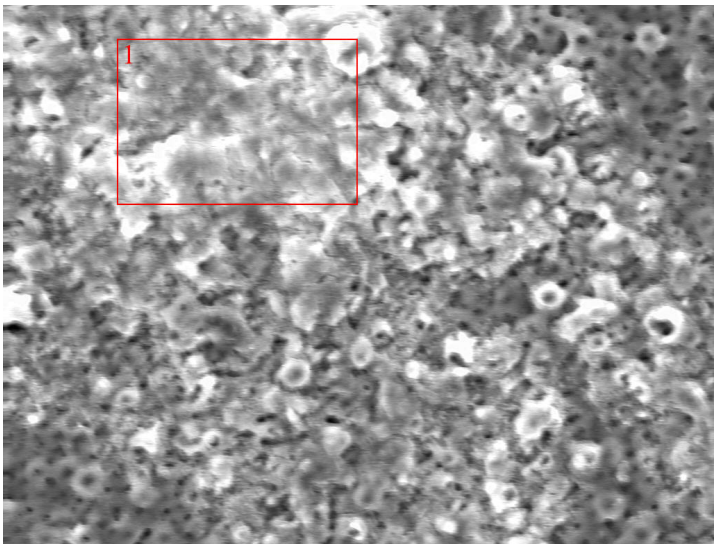

Figure 6.9 SEM images of electrolyte No. 2; 0.5 A 5 min. at 1000x magnification from a different region.

EDS analysis showed high Ca concentration in area (26.97% Ca, 27.47% Ti, 28.81% O) indicated in the inset shown in Figure 6.9. This was thought to be caused by the formation of $CaTi_4O_9$ compound in this region.

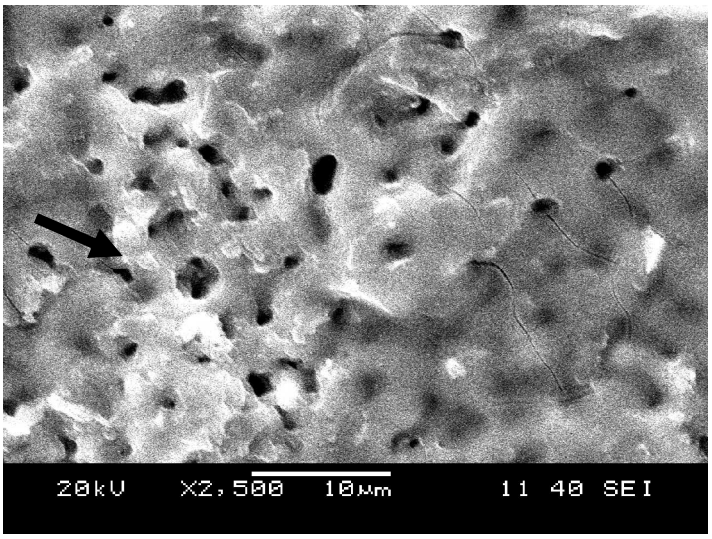

Figure 6.10 SEM images of electrolyte No.2; 2 A 2 min. at 2500x magnification.

Figure 6.10 shows that there are droplets near the pores of electrolyte No. 2 2A-2 min. surface. In MAO process, increase in current was thought to create droplets around the vicinity of the pores more than low current parameters. It was anticipated

that high current value causes electrophoretic effect for the particles to move towards the surface and accumulate on the film.

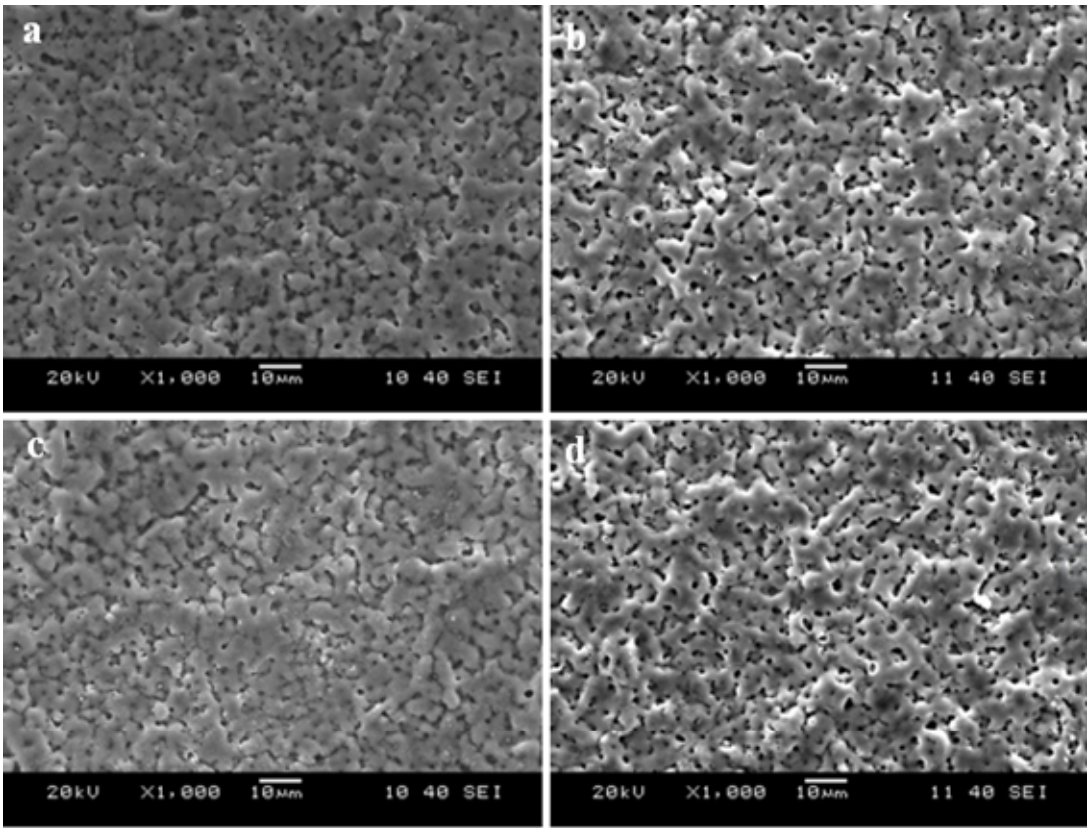

Figure 6.11 SEM image of samples treated in electrolyte No. 3. a) 0.5 A, 5 min. b) 1 A; 3 min. c) 2 A, 2 min. d) 1 A, 3 min. pre- coated with MgO

There were no difference in size and density of the pores with change in process current and time in electrolyte No. 3 as shown in Figure 6.11.

MgO pre-coating treatment, shown in Figures 6.11b and 6.11d, has not created any differences in morphological structure of the film produced in the electrolyte No.3.

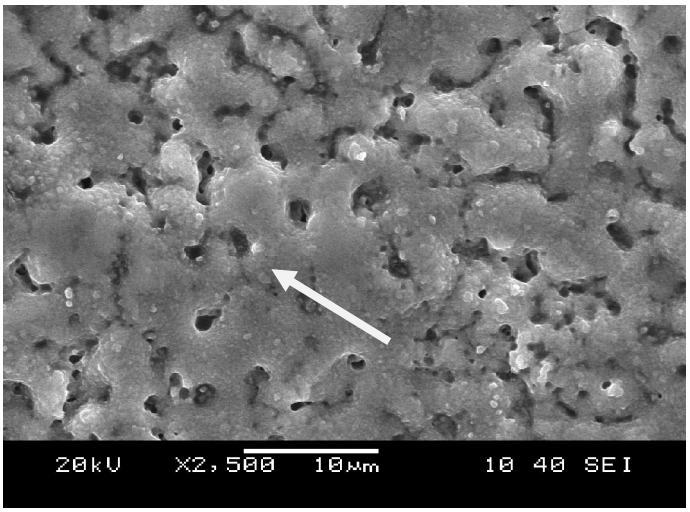

Figure 6.12 SEM images of electrolyte no. 3; 2 A 2 min. at 2500x magnification.

Figure 6.12 also shows droplets within the near vicinity of the pores obtained in electrolyte No.3, for 2A and 2 min. process. The same phenomenon has also observed in electrolyte No.2 for reasons already explained above.

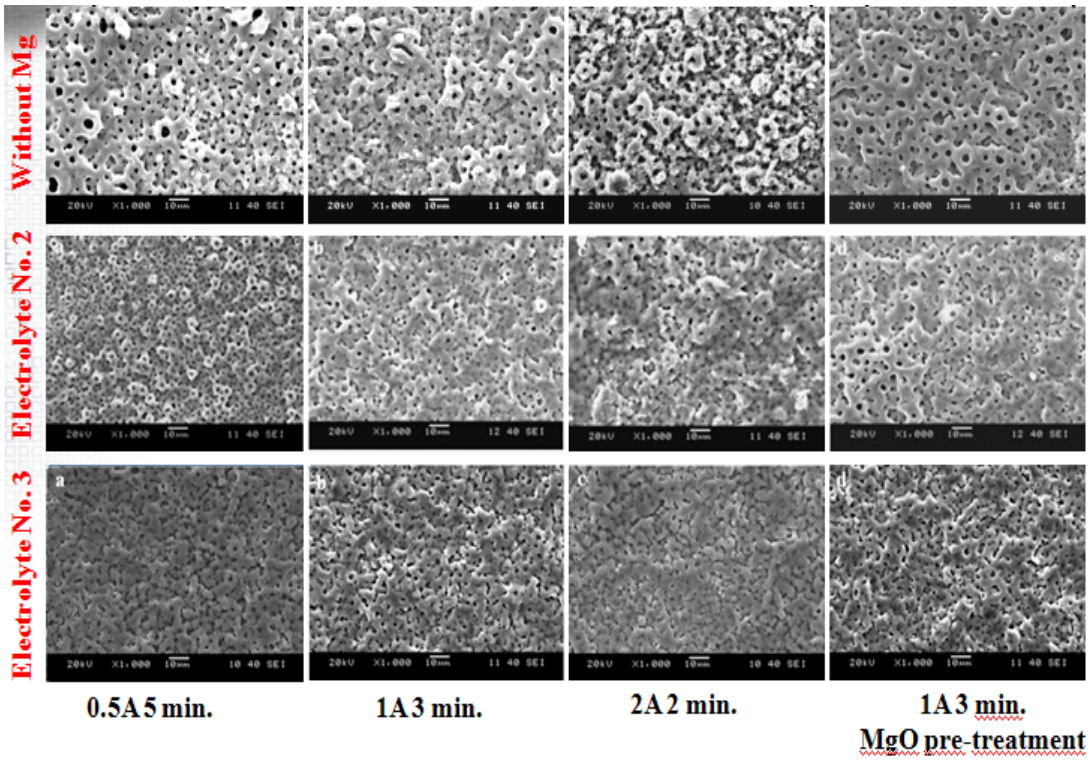

Figure 6.13 Comparison of SEM image of MAO samples treated in electrolyte without Mg, electrolyte No.2 and electrolyte No.3 a) 0.5 A, 5 min. b) 1 A; 3 min. c) 2 A, 2 min. d) 1 A, 3 min. pre- coated with MgO

Figure 6.13 gives the comparison of the morphology of the MAO coatings. Mg addition into the MAO electrolyte decreased the pore size and increased the pore density on the surface of samples. MgO pre-treatment before MAO created more homogenous morphology compared to the naked surface after MAO process.

6.4 EDS (Energy Dispersive Spectroscopy) Analysis of Coated Surfaces

Table 6.1 - 6.2 show the EDS analysis of 500x magnified surfaces treated with MAO process in electrolyte No.2 and No.3 with respect to process parameters.

Table 6.1 EDS analysis of MAO coatings which were obtained in electrolyte No.2

MAO parameters	**Mg**	Ti	O	**Ca**	P	V	Al
0.5A 5 min.	**2.35**	59.81	16.56	**7.58**	5.59	4.10	3.98
1 A 3 min.	**2.50**	56.27	17.94	**9.80**	5.56	4.35	3.56
2 A 2 min.	**2.42**	45.81	24.84	**15.43**	5.28	3.89	2.29
1A 3 min. (MgO pre-coating)	**2.38**	56.86	16.57	**11.56**	5.69	3.62	3.30

Table 6.2 EDS analysis of MAO coatings which were obtained in electrolyte No.3

MAO parameters	**Mg**	Ti	O	**Ca**	P	V	Al
0.5A 5 min.	**5.48**	53.63	23.05	**3.40**	6.79	4.05	3.55
1 A 3 min.	**5.59**	62.87	12.50	**3.70**	7.96	3.43	3.93
2 A 2 min.	**7.05**	56.55	16.27	**5.01**	8.50	3.70	2.89
1A 3 min. (MgO pre-coating)	**4.66**	60.71	16.33	**3.50**	7.53	3.70	3.53

EDS analysis of MAO treated surfaces showed that it's possible to dope Mg element into the oxide of Ti6Al4V by micro arc oxidation. Amount of Mg element can be enhanced using different MAO parameters. In two different electrolytes, maximum Mg concentration of surface is obtained in electrolyte No. 3 under 2A-

2min. condition (7.05%). Electrochemical deposition of MgO pre-coating was found to be not beneficial in MAO treatment in order to increase or control the Mg content of MAO films. Without pre-treatment, Mg content was found to have better manipulated with changing MAO bath composition and parameters. In the electrolyte No.2 and No.3, MgO pre-coating has decreased Mg element concentration of surfaces after MAO with respect to the naked surface for the same current and time parameter. Maximum Mg element concentration is obtained in electrolyte No. 3 under 2A, 2min. condition and was measured 7.05%. Electrolyte No.3 has less Ca concentration than electrolyte No.2 but all of them have the same Mg concentration. According to the EDS results of coatings which were obtained in electrolyte No.3, decreasing of Ca concentration in the MAO electrolyte caused Mg enhancement on the surface. That means shortage of calcium; magnesium took place of it on the surface.

6.5 XRD Analysis of Surfaces

Figure 6.14 – 6.15 show XRD analyses of the surfaces.

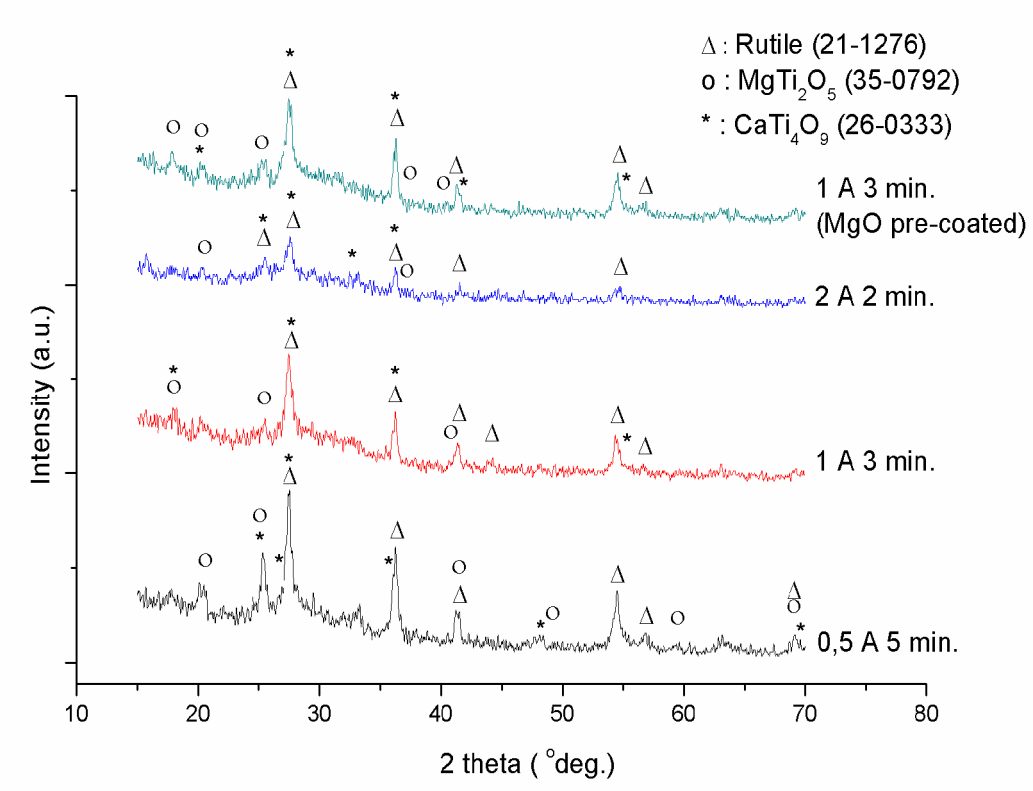

Figure 6.14 XRD analyses of electrolyte No. 2 group surfaces.

XRD analysis of samples treated in electrolyte No. 2 shows that TiO_2 (rutile), $MgTi_2O_5$ and $CaTi_4O_9$ phases have been fabricated by micro arc oxidation. Maximum peak intensity was observed under 0.5A, 5 min condition. Free energy of formation of $MgTi_2O_5$ according to the formula, $Mg+2Ti+5/2O_2$, at room temperature was given $\Delta G^o = -2.362$ MJ. The same energy of formation of $MgTi_2O_5$ according to the formula, $MgO+2TiO_2 \rightarrow MgTi_2O_5$, at higher temperature (1300-1400 °C) was reported to be -28±4 kJ (Brežnỳ B. & Muan, 1971), (Xirouchakis , Smirnov , Woody , Lindsley, 2002). Thus the formation of $MgTi_2O_5$ is expected to take place at large temperature intervals.

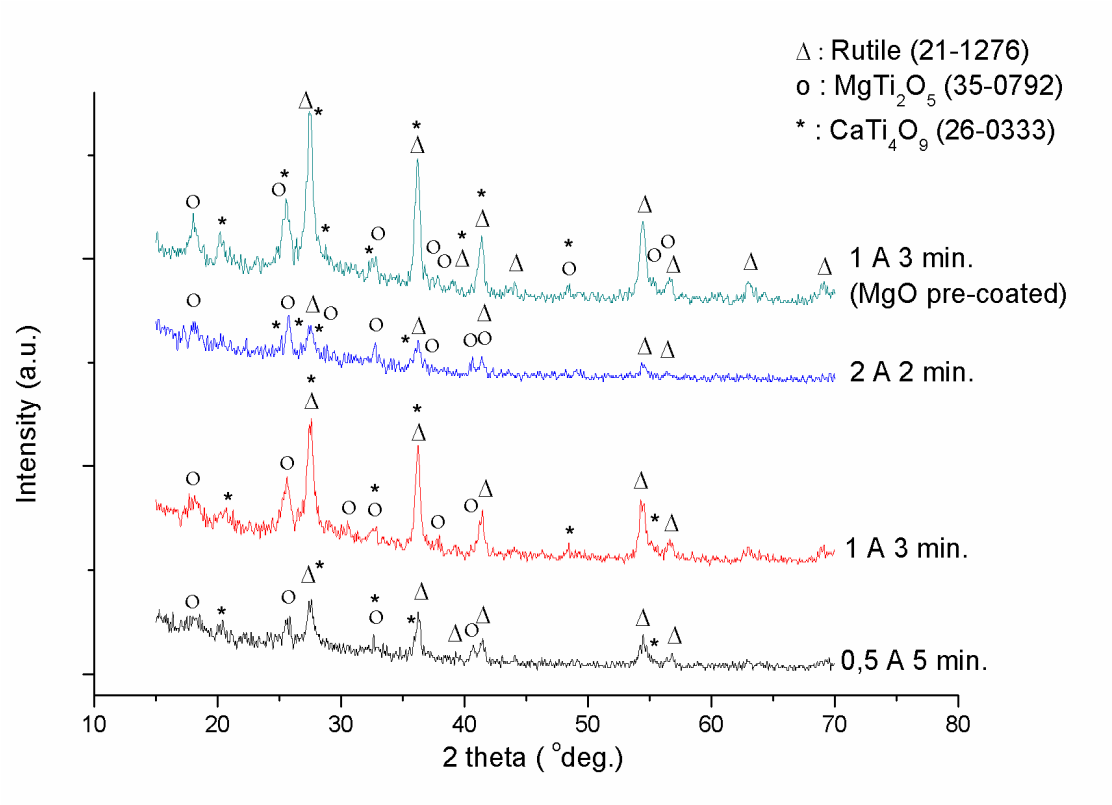

Figure 6.15 XRD analyses of electrolyte No. 3 group surfaces.

XRD analysis of MAO treated surfaces processed in electrolyte No. 3 shows that TiO_2 rutile, $MgTiO_5$ and $CaTi_4O_9$ spinal phases have been obtained. 1 A, 3 min MAO conditions used for MgO pre-coated samples created the maximum pick intensity among other test parameters studied.

The major phase of the MAO films are TiO_2 (rutile) in all samples. EDS data supported these XRD results.

6.6 Surface Roughness of Samples after Micro Arc Oxidation

Surface roughness of samples was measured by using XP2 profilometer. The results are given in Table 6.3.

Table 6.3 Surface roughness test result of the coatings

MAO Parameters	Electrolyte without Mg	Electrolyte No. 2	Electrolyte No. 3
0.5A 5 min.	0.380 μm	0.224 μm	0.248 μm
1A 3 min.	0.319 μm	0.292 μm	0.236 μm
2A 2 min.	0.397 μm	0.252 μm	0.245 μm
1A 3 min. (MgO pre-coated)	0.372 μm	0.272 μm	0.257 μm

Surface roughness was found to be independent of current or time. The results given in Table 6.3 indicate the importance of the electrolyte concentration. Thus the reaction of all electrolytes to same process parameter such as 0.5 A, 5 min. and 1A, 3 min indicated an increasing and decreasing roughness. Surface roughness was found to decrease under 1A, 3 min. compared to 0.5A 5 min. in electrolyte No.3. However the roughness has increased in the same current and time parameters in electrolyte No. 2. According to the results, Mg addition of electrolyte caused lower surface roughness. Surface roughness of an implant is an important factor for bone integration with host tissue. The higher the surface roughness becomes, the faster bone integration of an implant gets.

6.7 Electrochemical Characterization of Surfaces

Polarization resistance means the resistance of a material against corrosion. Polarization resistances of the surfaces were calculated using anodic and cathodic slope of Tafel curves of samples. The results are given in Table 6.4. ßa, ßc and i_{corr} values are used to measure polarization resistance according to following equation:

Table 6.4 Polarization resistances of surfaces.

MAO parameters	Polarization Resistance Values of Surfaces (Ω cm^2)	
	Electrolyte No. 2	Electrolyte No. 3
0,5A 5 min	70185	127495
1A 3 min	69285	120037
2A 2 min	105485	94681
1A 3 min (MgO pre-coated)	71007	70996

Polarization resistances of the surfaces have shown that, MAO parameters are effective for controlling dissolution properties of the surfaces in NaCl solution. Increase in current for MAO treatment seemed to have decreased polarization resistance indicating the increase in dissolution properties of the Mg-modified MAO film produced in electrolyte No.3.

6.8 Optical Micrographs of Samples After Corrosion Tests:

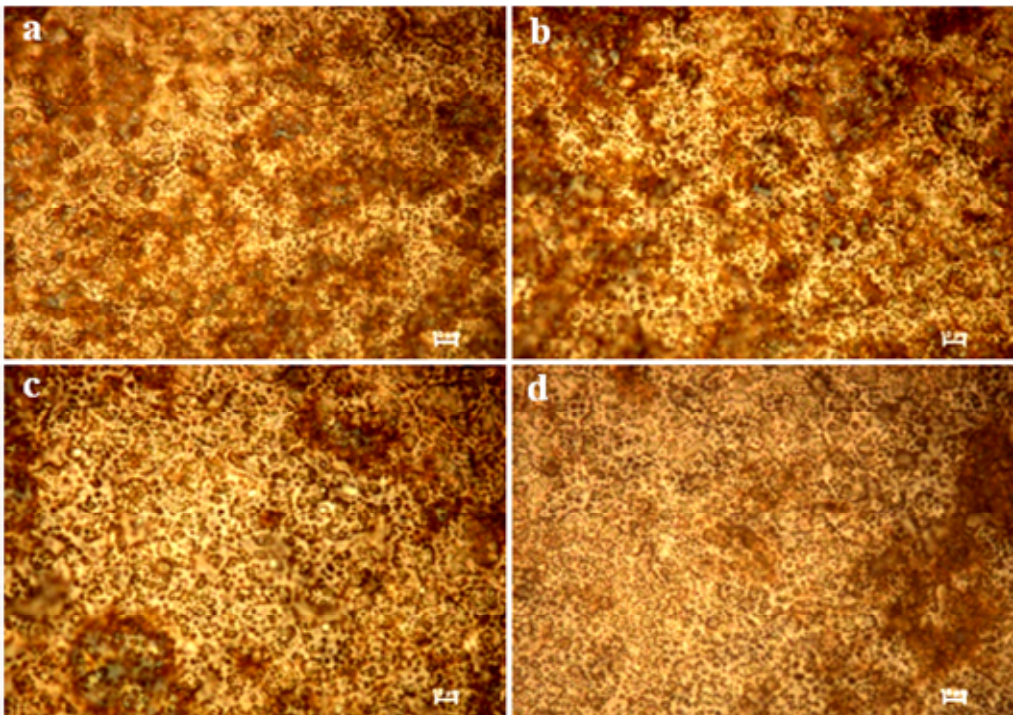

Figure 6.16 Optical pictures of electrolyte No. 2 group samples after corrosion test. a) 0.5A 5 min. b) 1A 3 min. c) 2A 2 min. d) 1A 3 min. MgO pre-coated.

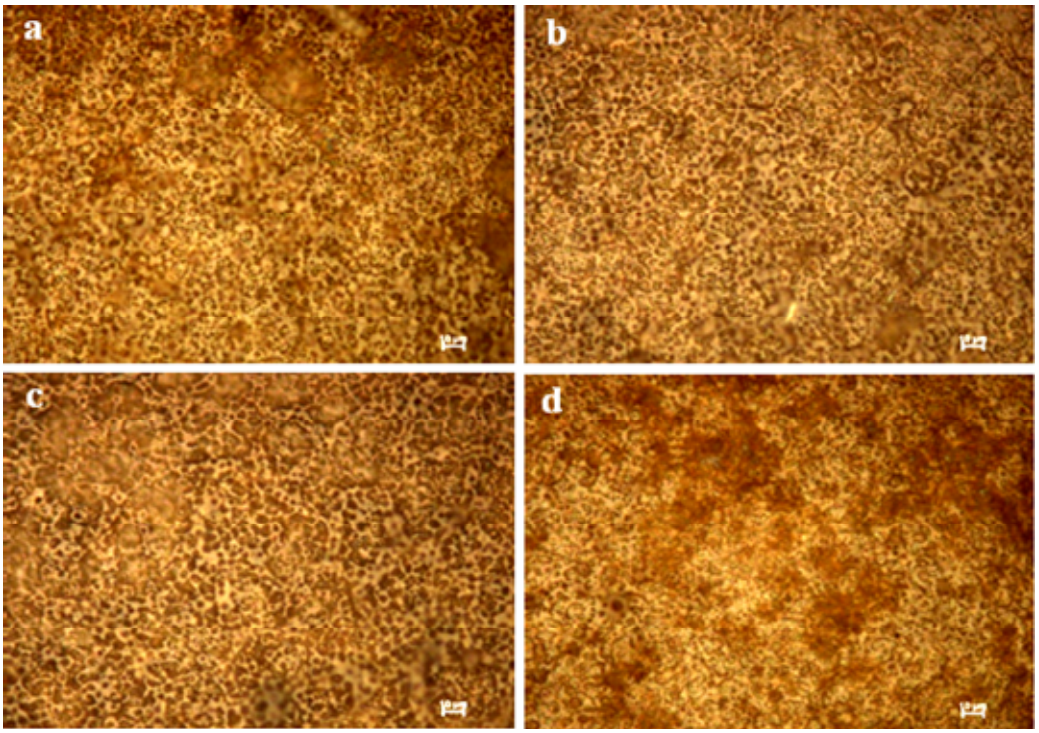

Figure 6.17 Optical pictures of electrolyte No. 3 group samples after corrosion test. a) 0.5 A 5 min. b) 1 A 3 min. c) 2 A 2 min. d) 1 A 3 min. MgO pre-coated.

Figure 6.16 – 6.17 show that there is no visible morphological difference in morphological structures between samples treated with different process parameters. All of surfaces are still porous after immersing NaCl solution.

CHAPTER SEVEN

CONCLUSIONS

7.1 General Results

1- For the electrolyte No.2, porosity decreased versus increasing current, structure changed into heterogen. MgO pre-coating did not create any morphological difference. At the parameter of 2A, 2 min. droplets occurred near the pores.

For the electrolyte No.3, there is no change of porosity versus current. MgO pre-coating process has no effect on morphology. There are droplets near the pores at 2A 2 min. Magnesium addition into MAO electrolyte decreased the pore size and increased the pore density.

2- Mg element was present in all of MAO treated oxide films structure. Maximum Mg concentration measured by EDS analysis as 7.05% was produced in electrolyte No.3 used with process parameters of 2A, 2 minutes. MAO processing conducted on electrochemically pre-coated MgO procedure created a lower concentration of Mg in the MAO films when compared to the samples without pretreatment. Under the same Mg concentration of 2 electrolytes, lack of calcium increased the magnesium concentration of coatings. That means magnesium took place of calcium.

3- Structures of MAO treated oxide films consisted of rutile (TiO_2), $MgTi_2O_5$ and $CaTi_4O_9$. Maximum pick intensity was detected at 0.5A, 5 min in the electrolyte No.2 and 1 A, 3 min in the electrolyte No.3.

4- In the electrolyte No.2, the lowest surface roughness 0.224 μm was obtained at MAO processing run at 0.5 A and 5 minutes. Other process parameter created no significant change in roughness. MgO pre-coating increased surface roughness successfully in the electrolyte No.3 with respect of all other process parameters studied. Compared to the electrolyte which does not include Mg, surface roughnesses of coatings were decreased in electrolyte No.2 and No.3.

5- Polarization resistances were found independent of current and time in the electrolyte No.2. MgO pre-coating process increased the polarization resistance

according to the naked surface for the same process parameters. In the electrolyte No.3, polarization resistance found to decrease with increasing current. MgO pre-treatment was found to be beneficial to decrease the polarization resistance compared to the naked surface.

6- After corrosion tests, all the MAO treated surfaces maintained the state of porosity. There were no observable morphological differences among the surfaces following corrosion tests.

7.2 Suggestion

Bioactivity tests of the fabricated surfaces should be carried out. For this purpose *in vivo* and *in vitro* tests can be applied. *In vitro* test are carried out using simulated body fluids (SBF). Before *in vivo* test, which is carried out inside of a living tissue, *in vitro* test of the surfaces should be completed. Simulated body fluids are prepared according to the ion concentration of human blood plasma. They can be used for not only evaluation of bioactivity of surfaces *in vitro*, but also biomimetic coating of apatites on various materials. Ion concentration of SBF solutions can be modified by addition of different chemicals. Ion concentration of SBF is given in Table 7.1.

Table 7.1 Ion concentration of SBF and human blood plasma (Kokubo and his friends, 1990).

ION	**Concentration (mmol/dm^3)**	
	Simulated body fluid (SBF)	**Human blood plasma**
Na^+	142.0	142.0
K^+	5.0	5.0
Mg^{2+}	1.5	1.5
Ca^{2+}	2.5	2.5
Cl^-	147.8	103.0
HCO_3^-	4.2	27.0
HPO_4^{2-}	1.0	1.0
SO_4^{2-}	0.5	0.5

To evaluate the bioactivity of a surface, SBF is applied at different pre-determined times. SBF can be renewed every day or kept constant during the test.

Incubators are used to keep the temperature of test media at 37ºC. After *in vitro* test, chemical and mechanical characterization techniques are applied to the surface such as XRD, EDS, SEM and scratch test. Evaluating the results of these analyses, bioactivity of a surface is determined.

REFERENCES

Assad M, Chernyshov AV, Jarzem P, Leroux MA, Coillard C, Charette S, & Rivard C-H. Porous titanium-nickel for intervertebral fusion in a sheep model: Part 2. Surface analysis and nickel release assessment. J Biomed Mater Res Pt B: *Appl Biomater*, 2003, 64B:121-129.

ASM (1978). *Sourcebook on industrial alloy and engineering data*. Metal Park, Ohio: American Society for Metals.

ASTM (2000). Annual book of ASTM standards. West Conshohocken, PA: ASTM

Benezra V, Mangin S, Treska M, Spector M, Hunter G, & Hobbs LW. Microstructural investigation of the oxide scale of Zr-2.5 Nb and its interface with the alloy substrate, in Biomedical Materials-Drug Delivery, *Implants and Tissue Engineering*, Mater Res Soc Symp Proc, 1999,550: 337-342.

Bernecki TF, ed. Thermal Spray Coating: Properties, Processes and Applications, *ASM International*: Materials Park, OH, 1992.

Bilgi A., Foresti E., Gregoriani R., Ripamonti A., Roveri N., Shah J. S., The role of magnesium on the structure of biological apatite, *Calcif. Tissue Int*., 50, s. 439-444, (1992).

Black, Levine, Jacobs (2007). Biomaterials overview. *The Adult Hip*. 2nd edition. (374-425). Philadlephia Pa: Lippincott Williams & Wilkins

Brežnỳ B. & Muan A1971, *Thermochim*. Acta 2 107

Bruesch P., Muller K., Atrens A. & Neff H. Corrosion of stainless steels in chloride solution –an XPS investigation of passive films, Appl. Phys., 1985, 38:1-18.

Buckwalter, Einhorn, Simon (2000). *Orthopedic Basic Science*. 2nd edition. (192-193). Rosemont: American Academy of Orthopedic Surgeons

Buser D., Schenk R. K., Steinemann S., Fiorellini J. P., Fox C.H., Stich H., Influence of surface characteristics on bone integration of titanium implants: A histomorphometric study in miniature pigs, *J. Biomed. Mater. Res*., 25, s. 889-902, (1991).

Cisse O, Savadogo O, Wu M, & Yahia LH. Effect on surface treatment of NiTi alloy on its corrosion behavior in Hanks' solution. *J Biomed Mater. Res.*, 2002, 61:339-345

Chen J., Shi Y., Wang L., Yan F., Zhang F., Preparation and properties of hydroxyapatite-containing titania coating by micro-arc oxidation, *Materials Letters*, 60, 20, s. 2538-2543, (2006).

Davis JR, ed. Metallic Materials, Chapter 3, in *Handbook of Materials for Medical Devices*, *ASM International*, Materials Park, Ohio, USA, 2003.

Davis J.R (2004). Coatings. *Handbook of Materials for Medical Devices*, p179-194.

Endo K., Araki Y., & Ohno H., *In vitro* and *in vivo* corrosion of dental Ag-Pd-Cu alloys, *Transaction of International Congress on Dental Materials*, 1989, 226-227.

Espostito M., Lausmaa J., Hirsch J. M., & Thomsen P., Surface analysis of failed oral titanium implants, *J. Biomed. Mater. Res. Appl. Biomater*., 1999, 48:559-568.

Filho J. T., Lidizio L. R., Sena L. A., Damasceno J.C., Achete C.A., Titanium oxide films produced by micro-arc oxidation for high performance titanium implants, XVIII IMEKO World Congress, Metrology for sustainable development, Rio de Janerio, Brazil, (2006).

Firstov GS, Vitchev RG, Kumar H, Blanpain B, & Van Humbeeck J. Surface oxidation of NiTi shape memory alloy. *Biomaterials*, 2002, 23:4863-4871.

Gledhill HC, Turner IG, & Doyle C. Direct morphological comparison of vacuum plasma sprayed and detonation gun sprayed hydroxyapatite coatings for orthopedic applications. *Biomaterials*, 1999, 20: 315–322.

Grainger S, ed. Engineering Coatings – Design and Applications, Abingdon Publishing: Oxford, 1989.

Groot K. D., Klein C. P. A. T., Wolke J. G. C., Blieck-Hogervorst J.M.A., Yamamuro T., Hench L.L., Wilson J., *Handbook of Bioactive Ceramics Vol. 2*, Calcium Phosphate and Hydroxylapatite Ceramics, CRC Press, Boca Raton, FL, s. 3, (1990).

Haasters J, v Salis-Salio G, & Bensmann G. The use of Ni-Ti as an implant in orthopaedics, in Deurig TW, Melton KN, Stockel D, & Wayman CM, eds. *Engineering Aspects of Shape Memory Alloys*, 1990, pp. 426-444

Han Y., Hong S.H., Xu K., Synthesis of nanocrystalline titania films by micro arc oxidation, *Materials Letters*, 56, s. 744-747, (2002).

Hanawa T., Titanium and its oxide film: a substrate for formation of apatite in the bone-biomaterial interface, ed. J. E. Davies, (University of Toronto Press, Toronto, (1991) pp:49-6I.

Hanawa T., Surface modification of Metallic Biomaterials. *Engineering materials for biomedical applications*. Toh Tuck Link: World Scientific.

Hanawa T., & Ota M., Calcium phosphate naturally formed on titanium in electrolyte solution, *Biomaterials*, I991, 12:767-774.

Hanawa T., Hiromoto S., Yamamoto A., Kuroda D. & Asami K., XPS characterization of the surface oxide film of 316L stainless samples that were located in quasi-biological environments, *Mater. Trans*., 2002,43:3088-3092.

Hanawa T., Hiromoto S., & Asami K., Characterization of the surface oxide filmof a Co-Cr-Mo alloy after being located in quasi-biological environments using XPS, *Appl. Surf. Sci*., 2001, 183:68-75.

Hanawa T., Hiromoto S., Asami K., Ukai H., & Murakami K., Surface modification of titanium utilizing a repassivation reaction in aqueous solutions, *Mater. Trans*., 2002, 43:3005-3009.

Hanawa T., Okuno 0., and Hamanaka H., Compositional change in surface of Ti-Zr alloys in artificial bioliquid, *J. Jpn. Inst. Met*., 1992, 56: 1 168-1 173.

Hanawa T. & Ota M., Characterization of surface film formed on titanium in electrolyte, *Appl. Surf. Sci*., 1992, 55:269-276.

Hanawa T., Takahashi H., Ota M., Pinizzotto R. F., Ferracane J. L., & Okabe T., Surface characterization of amalgams using X-ray photoelectron spectroscopy, *J. Dent. Res.*, 1987, 66:1470-1478.

Hao Y. L., Li S., Sun B. B., Sui M.L., Yang R., Ductile titanium alloy with low Poisson's ratio, *Phys. Rev. Lett*., 98, s. 216405-8, (2007)

Healy K. E. & Ducheyne P., The mechanisms of passive dissolution of titanium in a model physiological environment, *J. Biomed. Mater. Res*., 1992, 26:3 19-338.

S. Hobo & T. Iwata, Castable Apatite Ceramics as a New Biocompatible Restorative Material. I. Theoretical Considerations, *Quint. Int.,* Vol 16 (No. 2), 1985, p 135–141

Hubler G.K. & Hirvonen J.K., Ion-Beam-Assisted Deposition, *Surface Engineering,* Vol 5, *ASM Handbook,* ASM International, 1994, p 593–601

Ishizawa H., Ogino M., Formation and characterization of anodic titanium oxide films containing Ca and P, *J. Biomed. Mater. Res*., 29, s. 65–72, (1995).

Jin S. & Atrens A., ESCA- studies of the structure and composition of the passive film formed on stainless steels by various immersion times in 0.1 M NaCl solution, *Appl. Phys*., 1987, A42:149-165

Kapanen A, Ryhanen J, Danilov A, & Tuukkanen J. Effect of nickel-titanium shape memory alloy on bone formation. *Biomaterials*, 2001,22:2475-2480.

Kokubo T., Kushitani H., Sakka S., Kitsugi T., and Yamamuro T., Solutions able to reproduce *in vivo* surface-structure changes in bioactive glass-ceramic A-W, *J. Biomed. Mater. Res.,* 24, 721-734 (1990)

S. Kihara, A. Watanabe, and Y. Abe, Calcium Phosphate Glass-Ceramic Crown Prepared by Lost-Wax Technique, *Commun. Am. Ceram. Soc.,* Vol 67, 1984, p C100–C101

Kim M. S., Ryu J. J., Sung Y. M., One-step approach for nano-crystalline hydroxyapatite coating on titanium via micro-arc oxidation, *Electrochemistry Communications*, 9, s. 1886-1891, (2007).

LeGeros R. Z., Calcium phosphates in oral biology and medicine, Basel, Switzerland: *Karger AG*, (1991).

Li Y., Lee I., Cui F., Choi S., The biocompatibility of nanostructured calcium phosphate coated on micro-arc oxidized titanium, *Biomaterials*, 29, 13, s. 2025-2032, (2008).

Liu F., Wang F., Shimizu T., Igarashi K., Zhao L., Formation of hydroxyapatite on Ti–6Al–4V alloy by micro arc oxidation and hydrothermal treatment, *Surf. and Coat. Tech*., 199, 2-3, s.220-224, (2005).

Nie X., Leyland A., Matthews A., Deposition of layered bioceramic hydroxyapatite/TiO_2 coatings on titanium alloys using a hybrid technique of micro-arc oxidation and electrophoresis, *Surface and Coatings Technology*, , 125, 1-3, s. 407-414, (2000).

Nie X., Leyland A., Song H., Yerokhin A., Matthews A. Thickness effects on the mechanical properties of micro-arc discharge oxide coatings on aluminum alloys, *Surface Coatings Tech*., 116-119, s. 1061-1064, (1999).

Mitsuo Niinomi, Masaaki Nakai & Harumi Tsutsumi, (2010). Recent Development of high mechanical bio-functional metallic biomaterial, IMMC 2010*: The 15th International Metallurgical and Materials Congress*.

Park, Kim (2007). Metallic Implant Materials. *Biomaterials*. (16-38). New York: CRC Press

Percival M., Bone health & osteoporosis, Appl. *Nutr. Sci. Rep*., 5(4), s. 1-6, (1999).

Pham M. T., Reuther H., Matz W., Mueller R., Steiner G., Oswald S., Zyganov I., Surface induced reactivity for titanium by ion implantation, *J. Matter. Sci. Mater. Med*., 11, s. 383-91, (2000).

R.L. Moon & Y.-M. Houng, in chemical vapor deposition- *Principles and applications*, edited by M.L. Hitchman and K.F. Jensen (Academic Press, London, 1993)

Robert M. Pilliar (2009). Metallic Biomaterials. *Biomedical Materials*. (First Edition) (41-83) Chapel Hill: Springer

Plasma Technology Ltd, http://www.plasmatechnol.com/articleShow.asp?ArticleID=404, (2011).

Qu, N.S. Chan, K.C., & Zhu, D. (2004). Pulse co-electrodeposition of nano Al_2O_3 whiskers nickel composite coating, *Scripta Mater.,* 50, (8) 1131–1134.

Sarıtaş, (2004) . Paslanmaz Çelik Yassı Mamuller, 2. Baskı, 15-68.

A. P. Serro, A. C. Fernandes, B. Saramago, J. Lima, & M. A. Barbosa, Apatite desorption on titanium surfaces - the role of albumin adsorption, *Biomaterials*, 1997, 18:963-968)

Shi X. L., Wang Q. L., Wang F. S., Ge S. R., Effects of electrolytic concentration on properties of micro-arc film on Ti6Al4V alloy, *Mining Science and Technology*, 19, s. 220-224, (2009).

Shirkhanzadeh M., Calcium phosphate coatings prepared by electrocrystallization from aqueous electrolytes, *J. Mater. Sci. Mater. Med*., 6, s. 90-93, (1995).

Smith D.C., Pilliar R.M., Metson J.B. & Mclntyre N.S., Preparative procedures and surface spectroscopic studies, *J. Biomed. Mater. Res*., 1991,25:1069-1084.

Sundgren J. E., Bodo P., & Lundstrom 1., Auger electron spectroscopic studies of the interface between human tissue and implants of titanium and stainless steel, *J. Colloid Interface Sci*., 1986, 110:9-20.

Sundgren J. E., Bodo P., Lundstrom I., Berggren A., & Hellem S., Auger electron spectroscopic studies of stainless steel implants, *J. Biomed. Mater. Res*., 1985, 19:663-671

Teoh (2004). Introduction to biomaterials engineering and processing. *Engineering materials for biomedical applications*. Toh Tuck Link: World Scientific

Turner Irene G., Ceramics and Glasses, *Biomedical Materials*, (3-41), New York: Springer

Voevodin A. A., Yerokhin A., Lyubimov V. V., Donley M. S., Zabinski J. S., Characterization of wear protective Al-Si-O coatings formed on Al-based alloys by micro-arc discharge treatment, *Surf. Coat. Technol*., 86-87, s. 516–521, (1996).

Walczak J., Shahgaldi F., & Heatley F., *In vivo* corrosion of 316L stainless steel hip implants: morphology and elemental compositions of corrosion products, *Biomaterials*, 1998, 19:229-237.

Wang D. Y., Dong Q., Chen C. Z., Lei T.Q., Recent progress of micro-arc oxidation technique, *J. of the Chinese Cer. Soc*., 33(9), s. 1133-1138, (2005).

Wang Y., Nan K., Chen X., Ning C., Wang L., Zhao N., Characterization of bioactive ceramic coatings prepared on titanium implants by micro-arc oxidation, *Rare Metals*, 25, 1, s. 84-89, (2006).

Wever DJ, Veldhuizen AG, Sanders MM, Schakenrad JM, & Van Horn JR. Cytotoxic, allergic and genotoxic activity of a nickel-titanium alloy. *Biomaterials*, 1997, 18:1115-1120.

Xirouchakis D. Smirnov A, Woody K, Lindsley D H & Anderson D J 2002 *Am. Mineral*. 87 658

Yerokhin A. L., Nie X., Leyland A., Matthews A., Dowey S. J., Plasma electrolysis for surface engineering, *Surf. Coatings Tech*., 122, s. 73–93, (1999).

Zardiackas LD, Parsell DE, Dillon LD, Mitchell DW, Nunnery LA, & Poggie R. Structure, Metallurgy and mechanical properties of a porous tantalum foam. *J Biomed Mater Res (Appl Biomater),* 2001, 58: 180-187.

Zhang Y. X., Han Y., Huang P., Sun J. F., Xu K. W., Adhesive strength and bioactivity of titania films prepared by micro-arc oxidation, *J. of the Chinese Cer. Soc*., 32(2), s. 122-126, (2004).

Zhao Y. F., Yang S. Y., Han M. W., Technique of plasma micro arc oxidation and its development, *Materials Review*, 6, s. 102-104, (2006).